Physics – Uspekhi **68** (8) 785 – 806 (2025)

CONFERENCES AND SYMPOSIA

PACS numbers: **95.30. – k,** 97.60.Bw, 98.70.Sa

ON THE 100th ANNIVERSARY OF S.I. SYROVATSKII'S BIRTH

Supernovae as sources of cosmic rays *

A.M. Bykov

DOI: https://doi.org/10.3367/UFNe.2025.03.039956

Contents

Abstract. The enormous energy release during supernova outbursts and observations of non-thermal radio emission allowed V.L. Ginzburg and S.I. Syrovatskii to substantiate more than 60 years ago the hypothesis about the key role of supernovae as sources of the main component of galactic cosmic rays. To date, multichannel observations of supernova remnants in the entire electromagnetic wavelength range have provided a wealth of data confirming the reality of proton and electron acceleration to energies of the order of 100 TeV. Several questions remain to be solved, including the problem of the origin and search for sources of the observed high-energy cosmic rays in the range from 100 TeV to 1000 PeV. Solving the problems of efficient conversion of the kinetic energy of supernova ejecta, the rotational energy of pulsars, and the energy of anisotropic plasma flows around accreting black holes into a population of relativistic particles invites kinetic simulations of nonlinear mechanisms with a broad dynamic scale range. Simulations are necessary to determine the highest energies of particles accelerated by super-Alfvenic plasma flows with frozen-in magnetic fields and collisionless shock waves. The task is to reveal the physical mechanisms of strong (superadiabatic) enhancement of magnetic turbulence required for rapid particle acceleration by the Fermi mechanism. The review presents the results of kinetic simulation and analysis of nonlinear production mechanisms of strong anisotropic magnetic turbulence and accelerated particle spectra. Recent observations of polarized X-ray synchrotron radiation from supernova remnants Tycho Brahe, Cassiopeia A, SN1006, etc. with the IXPE (Imaging X-ray Polarimetry Explorer) orbital observatory have made it possible to look inside cosmic particle accelerators using nonlinear models and understand the modification mechanisms of strong shock waves. Also discussed are the possibilities of acceleration of cosmic ray nuclei by powerful anisotropic plasma outflows in compact relativistic remnants of collapsed supernovae. Young pulsars in binary star systems, as well as accreting black holes — microquasars — can accelerate nuclei to energies significantly above a PeV.

Keywords: supernovae, cosmic rays, pulsar nebulae, binary gamma-ray sources, particle acceleration mechanisms, polarized X-ray radiation

1. Introduction

Experiments involving balloons to accurately measure the level of ionization of the atmosphere in relation to the altitude above Earth, which were performed by the young Austrian physicist Victor Hess in 1911–1913 [1], led to the discovery of ionizing radiation of extraterrestrial origin. In 1925, Robert Millikan called this extraterrestrial radiation 'cosmic rays' (CRs). Experiments to study cosmic rays with a Wilson chamber placed in a magnetic field at LPTI (now Ioffe Institute) in 1927–1929 allowed D.V. Skobeltzyn to find that cosmic rays were high-energy charged particles [2, 3]. Using the open natural cosmic particle accelerator made it possible to obtain many fundamental results in particle physics. These

A.M. Bykov
Ioffe Institute, Russian Academy of Sciences,
ul. Politekhnicheskaya 26, 194021 St. Petersburg, Russian Federation
E-mail: byk@astro.ioffe.ru, byk.astro@mail.ioffe.ru

Received 30 June 2025
Uspekhi Fizicheskikh Nauk **195** (8) 835 – 857 (2025)
Translated by E.N. Ragozin

* The review is based on a talk given at the Scientific Session of the Physical Sciences Division of the Russian Academy of Sciences on 5 March 2025 (see *Phys. Usp.* **68** (8) 745 (2025); *Usp. Fiz. Nauk* **195** (8) 793 (2025).

results include the experimental discovery of the positron and the muon by Carl Anderson [4]. Before the construction of modern accelerators and colliders, much experimental data in particle physics was obtained from the study of cosmic ray interactions. [1] The problem of the origin of cosmic rays was hard to resolve proceeding from optical astronomy data alone, which were available in the first half of the twentieth century.

In 1934, Mount Wilson Observatory astronomers W. Baade and F. Zwicky, relying on an analysis of optical observations, suggested that the supernova phenomenon accompanied the transition of an ordinary star into a compact object of smaller mass. They estimated the energy release of a supernova at $\sim 3 \times 10^{51}$ erg (for a radius of the radiating black body of about 3×10^{13} cm) and came up with an important hypothesis about the relation between cosmic rays and supernova outbursts [8]. The development of radio astronomy in the late 1940s made it possible to observe nonthermal emission of cosmic ray electrons and positrons in their probable sources (see the review of the development of radio astronomy in Ref. [9]). The first extrasolar radio source was discovered in 1948 in the Crab Nebula, a remnant of the supernova of 1054. Nonthermal spectra of diffuse radio emission from the Galaxy and the observed polarization of the Crab Nebula radiation were indications of synchrotron radiation by relativistic electrons in such systems [10, 11]. Observations proved the widespread occurrence of the electron component in CRs and the presence of high-power sources of accelerated electrons outside the solar system (in particular, supernova remnants) [12]. For a quantitative analysis of observations of nonthermal radiation, V.L. Ginzburg and S.I. Syrovatskii constructed a consistent theory of cosmic sources of polarized synchrotron radiation. This theory took into account the evolution of the spectra of radiating electrons and positrons under the influence of energy losses and particle transfer in the sources. It was established that relativistic electrons in radio sources are of primary origin and are not a product of inelastic interactions of CR nuclei. Furthermore, indications were obtained of a rapid particle exchange between spiral arms and radio halos [13]. Constructed more than 60 years ago, the theory of synchrotron radiation of cosmic electron ensembles [14, 15] is widely used today to model synchrotron radiation in the entire energy range of the electromagnetic spectrum, up to gamma rays, which are observed from the Crab Nebula by orbital telescopes [16, 17].

Radio observations performed in the late 1940s demonstrated the widespread occurrence of relativistic electrons in the Galaxy, which was consistent with the hypothesis of a possible relation between supernovae and cosmic rays. The question reduced to the search for mechanisms for accelerating particles to ultrarelativistic energies and to the statistics of supernovae as probable sources of CRs. Observations of relativistic nuclei and electrons of cosmic rays on Earth and relativistic electrons in the Galaxy called for the development of cosmic ray acceleration mechanisms in sources of different types. As an alternative to Edward Teller's assumptions about the localization of the sources of the observed cosmic rays in the solar system, Enrico Fermi proposed in 1949 [18] a mechanism for accelerating charged particles by way of their multiple scattering by large-scale fluctuations of the magnetic field (magnetic clouds) moving at random speeds in the interstellar medium of the Galaxy. The Fermi acceleration mechanism and its development in the context of CR acceleration in supernova remnants is discussed in Section 5.1.

Modeling the acceleration of relativistic charged particles due to the transfer of energy of large-scale plasma motion to them in CR sources, as well as modeling the CR transport in galaxies, invite a description of electromagnetic fields of different scales. A feature of cosmic plasma is its high conductivity, which leads to the freezing of the magnetic field into plasma flows and to the absence of an electric field in the rest frame of the moving plasma element. The specified plasma properties made it possible to formulate the equations of magnetohydrodynamics (MHD), capable of describing large-scale motion of cosmic plasma together with the evolution of its magnetic fields [19].

S.I. Syrovatskii [20] formulated a closed system of MHD equations in the form of conservation laws, which made it possible to naturally classify possible types of discontinuity surfaces of MHD flows, as well as to study the stability problems of shock waves (SWs) and tangential discontinuities. Shock waves are formed by supersonic outflows in the form of winds and jets and accompany a powerful release of energy in flare events. Therefore, SWs are of key importance for the CR acceleration by cosmic plasma motion. The change in the energy of cosmic ray particles in flows of highly conductive cosmic plasma is caused by induction electric fields. The electric field in the laboratory frame of reference, $\mathcal{E} = -(\mathbf{u}/c) \times \mathbf{B}$, is determined by the local values of the plasma velocity $\mathbf{u}(\mathbf{r}, t)$ and the magnetic field strength $\mathbf{B}$. The work of the electric field during the reversal of the particle with velocity $\mathbf{v}$ by a magnetic field leads to a change in the energy of the particle E [13],

$$\Delta E = -2E \frac{\mathbf{uv}}{c^2}\,, \tag{1}$$

corresponding to the law of elastic reflection of a particle by moving clouds in the Fermi mechanism. Analysis of the process of particle acceleration by low-frequency electromagnetic fields (with frequencies below the gyrofrequency of background plasma ions) in the MHD approximation led the authors of Refs [13, 14] to the conclusion that relatively rapid regular particle acceleration based on relation (1) is, in essence, an adiabatic compression, and therefore it is limited in magnitude by the permissible increase in the plasma density in the accelerator. By contrast, stochastic Fermi acceleration is significantly slower, but the associated increase in particle energy over a long time is limited only by energy losses and the escape of particles from the acceleration region.

In the early 1960s, the analysis of observational data on the spectrum, anisotropy, and chemical and isotopic composition of cosmic rays in combination with the analysis of radio astronomical observations, allowed V.L. Ginzburg and S.I. Syrovatskii to formulate the basic provisions of the theory of the origin of cosmic rays and to construct a quantitative model of the propagation and transformation of the chemical composition of CRs [13, 14]. For the quasi-stationary model, the power of CR sources in the Galaxy with a large halo radius of $\gtrsim 10$ kpc was estimated at 3×10^{40} erg s^{-1}. Supernova outbursts and, as expected, outbursts in the galactic center provide a power source sufficient to form and maintain in the Galaxy the main population of CRs with energies up to $\sim 10^{15}$ eV. On the

[1] A very fascinating history of the discovery of cosmic rays and their early investigators can be found in Refs [5–7, 26].

other hand, the energy estimates of particles accelerated in nonexploding stars did not exceed $\sim 10^{13}$ eV, and the total power of such sources, according to the authors of the theory, was insufficient. Note that at that time energetic pulsars, microquasars, and compact clusters of young massive stars had not yet been discovered. It was assumed that higher-energy particles came to the Galaxy from extragalactic sources, in particular from powerful radio galaxies. The model successfully separated the so-called *external problem* (i.e., CRs outside the sources) and *internal problem* (CRs in the sources). To solve the external problem, it was shown that CR transport in the disk and halo of the Galaxy, described by diffusion-type equations taking into account the motions of the medium and various types of losses, determines the transformation of the CR composition and the observed abundance of secondary particles. The authors of the theory emphasized the importance of searching for CR sources as well as verifying and developing the theory itself by means of gamma-ray astronomy [24, 25].

The past years have confirmed the validity of the basic principles of the theory. These principles still stand up to scrutiny by modern precision observations of CRs (and processes involving them) in ground-based and orbital experiments (which are now all-wavelength, including high-energy neutrinos) [26–33]. Observations of cosmic ray sources by modern X-ray and gamma observatories, both orbital and ground-based atmospheric Cherenkov telescopes, play a significant role in verifying and refining the theory of the origin of CRs. In this field, very interesting results have been obtained over the past 20 years.

This review is concerned with the *internal problem* (in the terminology of Ginzburg and Syrovatskii), i.e., the problem of studying the particle acceleration mechanisms in supernova remnants considered to be particle accelerators and sources of high-energy radiation and cosmic rays. In this case, we will consider supernova remnants in a broad sense, including pulsars and accreting black holes. One of the important and open questions today is the origin of CR nuclei in the $10^{15}-10^{18}$-eV energy range, where the contribution of relativistic stars (in particular, microquasars) produced in the collapse of the cores of massive stars included in binary star systems is possible. The main observational data on cosmic rays are summarized in Section 2. Section 3 briefly discusses the main data on the properties and statistics of supernovae and their remnants that are significant for the problem of the origin of CRs. Discussed in Section 5 are particle acceleration mechanisms as applied to supernova remnants. An analysis of observations of nonthermal radiation from supernova remnants is outlined in Section 6. Discussed in Section 7 are the modeling of and search for galactic sources of particles with energies of the order of and above 10^{15} eV (i.e., PeV-energy particles).

This review is a slightly expanded version of the report presented at the Scientific Session of the Physical Sciences Division of the Russian Academy of Sciences on March 5, 2025. This RAS session was dedicated to the centenary of the birth of Sergei Ivanovich Syrovatskii (1925–1979). Sergei Ivanovich's ideas, which he generously shared, stimulated the research of many of his colleagues, including the author of this paper, in a number of fields of astrophysics. Figure 1 shows a photograph of a discussion at the Leningrad Seminar on Cosmophysics (1972), where S.I. Syrovatskii debated Richard Lingenfelter, one of the active researchers of cosmic ray sources [33].

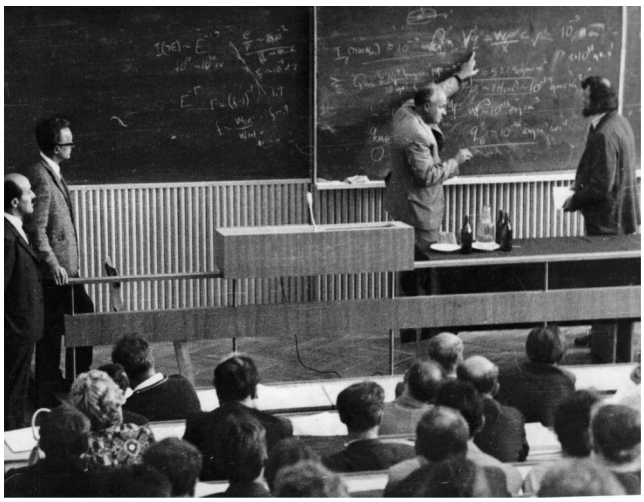

Figure 1. Discussion on problems of cosmic ray origin at Leningrad Seminar on Cosmophysics in 1972, in auditorium of Polytechnic Institute. In center at the board is S.I. Syrovatskii (Lebedev Physical Institute) discussing issues with R. Lingenfelter (University of California).

2. Cosmic rays in the Galaxy

Figure 2 shows the spectrum of all CR nuclei observed in terrestrial orbit in relation to particle energy (per nucleon). The spectrum was obtained from an analysis of a set of data from long-term observations of extensive air showers formed by high-energy cosmic rays interacting with Earth's atmosphere. The observations were made using the ground-based installations listed in Fig. 2.

Significant data on the spectra and composition of primary and secondary CRs at energies below 10 TeV were obtained using the balloon and orbital particle detectors DAMPE, AMS-02, CALET, etc. [34–36]. Measurements of the spectrum of all nuclei in the energy range from 10 TeV to 1 PeV by the HAWC (High Altitude Water Cherenkov) observatory [37} revealed recently a kink-like feature of the spectrum. This kink is located at the energy of $40.2^{+1.0}_{-1.0}$ (stat.) $^{+6.2}_{-6.4}$ (syst.) TeV, where the spectral index softens from $2.53^{+0.01}_{-0.01}$ (stat.) $^{+0.04}_{-0.05}$ (syst.) to $2.71^{+0.01}_{-0.01}$ (stat.) $^{+0.03}_{-0.04}$ (syst.).

One of the most important observational result in high energy CR physics was the discovery in 1958 by G.V. Kulikov and G.B.Khristiansen [38] of the so-called knee in the region of particle energies of the order of PeV. This discovery was made on the basis of an analysis of the characteristics of extensive air showers. This kink is marked in Fig. 2 as the *first knee* (knee in Fig. 2). The high sensitivity of the LHAASO detectors has recently made it possible to study the features of the CR spectrum and composition in the region of the first knee with unprecedented accuracy.

Analysis of the data from observations of the spectrum and the average logarithm of the particle mass in the 0.3–30-PeV energy range obtained at the LHAASO-KM2A facility from September 2021 to December 2022 allowed determining the position of the knee in the energy spectrum of all particles as 3.67 ± 0.05(stat.) ± 0.15(syst.) PeV [39]. The spectral index of CRs before the break was determined as -2.7413 ± 0.0004(stat.) ± 0.0050(syst.) and above the break as -3.128 ± 0.05(stat.) ± 0.027(syst.). The average logarithm of the atomic weight, $\langle \ln A \rangle$, turned out to be greater than that of helium in the entire measurement range; in the range of 0.3–3 PeV, it decreases and then begins to increase. Since the

behavior of $\langle \ln A \rangle$ changes precisely at the energy of the spectrum kink, the authors of Ref. [39] concluded that the break in the spectrum of all particles is probably due to the kink in the spectrum of the light component. Furthermore, the LHAASO observations made it possible to separately measure the proton spectrum in the 0.15–12-PeV range. It was shown that the proton spectrum first becomes harder in the range from 0.15 to 3 PeV, and then, above 3 PeV, it becomes significantly softer [40]. The authors of the observations concluded that there is a separate CR component in the energy range of the order of 100 PeV, probably related to gamma-ray sources of the PeV energy range observed by LHAASO [41]. Significant estimates of the kink energies in the proton spectrum (~ 4.4 PeV) and in the helium spectrum (~ 11 PeV) were obtained by applying machine learning methods to the KASCADE experiment data in Ref. [42]. The kink energies are compatible with the dependence of their position on the particle rigidity parameter. Observations of high-energy CR anisotropy indicate a change in the nature of the dependence of the angular anisotropy amplitude on the particle energy in the PeV range. The amplitude of the CR anisotropy with energies of $\gtrsim 11$ PeV begins to increase with increasing particle energy (see, for example, Ref. [43]). So, there is observational evidence that the first knee in the spectrum is probably due to kinks in the spectra of protons and the light CR component.

Published recently were the results of LHAASO observations of diffuse gamma-ray radiation with photon energies from 10 TeV to 1 PeV in the galactic plane [44]. The fluxes of diffuse gamma-ray radiation with energies above 10 TeV were measured with a significance of 29.1 σ from the inner region of the Galaxy ($15° < l < 125°, |b| < 56°$), and with a significance of 12.7 σ from the adjacent region ($125° < l < 235°, |b| < 5°$). The spectral indices in both regions were estimated at -2.99. The measured absolute fluxes in the 10–60-TeV photon energy range significantly (by several-fold) exceed the predictions of the models constructed by the authors of Ref. [44] based on the CR terrestrial in-orbit spectrum measurements, the distribution of interstellar gas, and the cross sections of hadron interactions. The difference obtained may arise from the existence of an additional population of sources whose contribution was not included. Another explanation may be due to the possible nonuniformity of the distribution of high-energy CRs in the Galaxy.

On the other hand, a comparison of the results of subsequent modeling performed in Refs [45, 46] revealed a noticeable disagreement with the conclusions of Ref. [44]. The authors of Ref. [45] took into account the uncertainties in the parameters of the diffuse gamma-ray model and came to an agreement between this model and the measurement data of Ref. [44] without involving an additional population of radiation sources. The calculations of gamma-ray fluxes in Ref. [46], which were performed on the basis of the measured LHAASO spectra of PeV protons [40], yielded higher gamma-ray fluxes than those measured by LHAASO both in the inner and in the neighboring region ($125° < l < 235°$, $|b| < 5°$). Taking into account some uncertain factors of the model (such as the absorption of gamma-ray photons due to the production of electron-positron pairs during γ–γ scattering by the background infrared microwave radiation of the Galaxy or the spatial nonuniformity of the distribution of PeV-range CRs) could reduce the model gamma-radiation flux. The hypothesis of the homogeneity of the distribution of high-energy CRs can be verified by measuring the gamma-radiation fluxes in different directions. In the case of a uniform CR distribution, after correction for absorption effects, the angular distribution of the radiation should be the same at different energies. Such a test of the uniformity of the distribution of PeV-range CRs in the galactic disk by observations by the LHAASO observatory can be expected in the coming years.

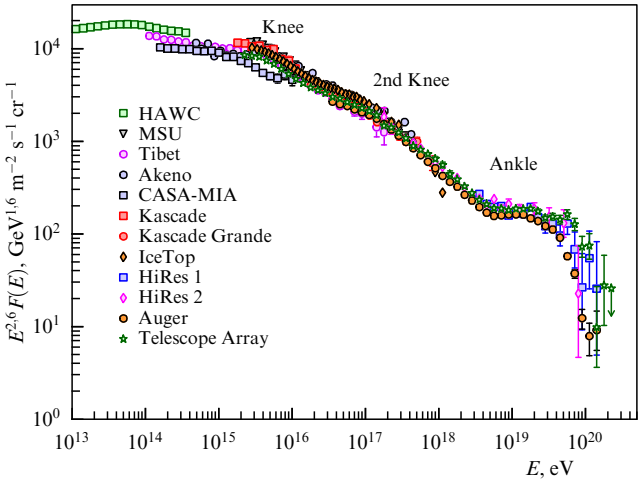

Figure 2. Spectrum of all CR particles as a function of particle energy (per nucleon), which was obtained from a set of observations of extensive air showers. Spectrum is borrowed from the work of P.A. Zyla et al. (Particle Data Group) *Progr. Theor. Exp. Phys. Supplemental material*, 083C01 (2020).

The data available today indicate the possibility of the presence of an additional component of galactic CRs in the vicinity of the spectrum kink. This component could also contribute at energies above PeV — up to the energies of the second knee, indicated in the spectrum in Fig. 2. The energy density of CRs with energies above E decreases faster than $E^{-0.6}$. Therefore, to maintain the observed intensity of CRs with $E \gtrsim 100$ PeV, in all likelihood, a power of galactic sources of the order of 10^{39} erg s^{-1} is sufficient. The power estimate depends on the uniformity of the CR distribution, the model of high-energy particle transport, and the size of the CR halo of the corresponding energies.

The collection of results of observations of the spectrum and $\langle \ln A \rangle$ for CRs with energies above PeV are shown in Fig. 3, which was borrowed from Ref. [21]. The CR spectra and the results of measurements of the average chemical composition (atomic number) of nuclei with energies above 100 TeV were obtained by Tunka 25 and 137, Kascade Grande, and IceTop ground-based observatories. The observations indicate the presence of features in the CR spectrum, which may indicate contributions from particle accelerators of a different nature. Despite the noticeable quantitative difference between the data of the listed experiments and the Tale results (also shown in Fig. 3), the set of all available observations does not contradict the hypothesis of a change in the average CR mass composition from light to heavier in the energy range between a PeV and 100 PeV. A detailed analysis of a large volume of KASCADE experiment data and a study of systematic uncertainties in the IceTop, Tale, and LHAASO data sets, which was performed in Ref. [42], testified to the compatibility of the $\langle \ln A \rangle$ estimates in these experiments. The data on measuring the extensive air shower density $X_{\max}$ in the energy range from 100 to 300 PeV by the LOFAR radio telescope led the authors of Ref. [47] to the conclusion that

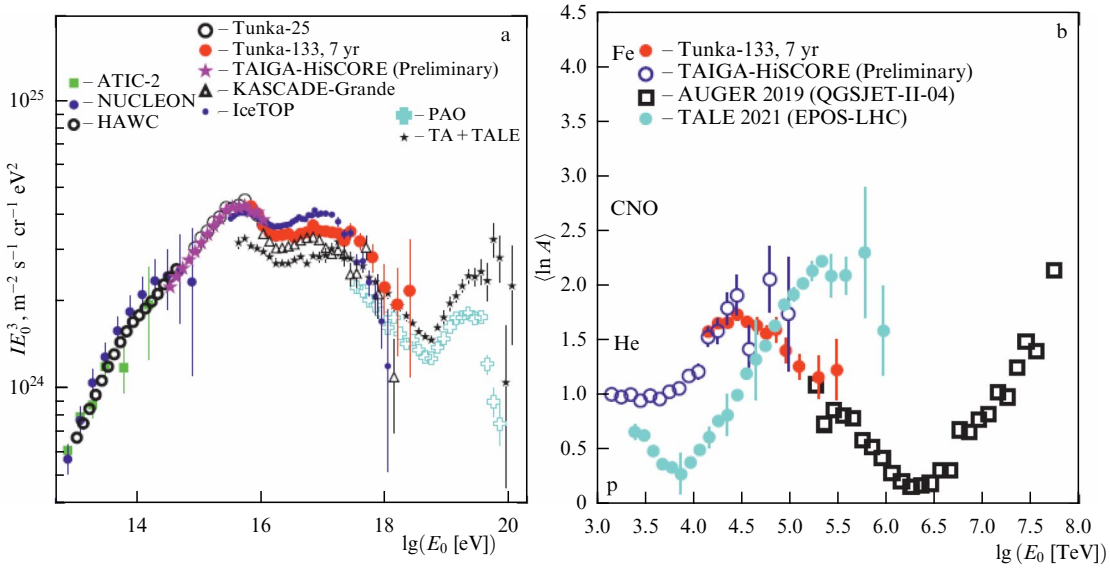

Figure 3. (a) Results of observations of the spectrum of all cosmic ray particles with energies above PeV. (b) Logarithm of the mass number of nuclei, $\langle \ln A \rangle$, versus the energy of nuclei, characterizing the change in the chemical composition of CRs [21].

$\sim 80\%$ of the particles in this energy range are protons and helium nuclei, which may mean that there are populations of galactic CR sources with the highest accelerated proton energies of the order of several PeV, which make a significant contribution to the CR nuclei fluxes in the energy range between PeV and 100 PeV. With a power of such sources of the order of 10^{39} erg s^{-1}, they can support a population of galactic CRs with energies above PeV.

Questions about the nature of the two kinks in the CR spectrum in Fig. 2, about the CR sources and the propagation of particles with energies in the PeV range, as well as about the transition between the galactic and metagalactic CR components [48], remain largely open, although the volume and quality of the new data outlined above give grounds for hope for progress in the near future. We will now discuss possible high-energy CR accelerators in the Galaxy that contribute to the observed CR spectrum.

To understand the criteria for selecting possible sources of high-energy CRs, it is convenient to start with the model estimate of the maximum energy $E_{\max}$ of a particle with charge Z accelerated by the flow of plasma with a frozen magnetic field and a magnetic energy flux density (per unit solid angle) $\mathcal{L}_{\mathcal{M}}$:

$$E_{\max} \approx 2 \times 10^{17} Z \frac{\phi(\beta_{\rm f}) \mathcal{L}_{40}^{1/2}}{\Gamma_{\rm f}} \text{ eV}. \qquad (2)$$

Here, $\mathcal{L}_{40}$ is the *magnetic luminosity* expressed in units of 10^{40} erg s^{-1}, and $\beta_{\rm f} = u_{\rm f}/c$ and $\Gamma_{\rm f} = 1/(1-\beta_{\rm f}^2)^{1/2}$ are the dimensionless velocity and the Lorentz factor of the MHD flow, respectively. In the case of an ultrarelativistic flow ($\Gamma_{\rm f} \gg 1$), the function $\phi(\beta_{\rm f}) \to 1$. For nonrelativistic flow velocities $\beta_{\rm f} \ll 1$, we have $\phi(\beta_{\rm f}) \propto \beta_{\rm f}^{1/2}$ [49]. This estimate does not include the particle energy loss due to radiation and inelastic destruction mechanisms, which is usually applicable to accelerators of nuclei in the PeV energy range. The derivation of relation (2) relies on the assumption that the particle acceleration time is shorter than the dynamic time of the flow (see Ref. [49]). For a given value of the *magnetic luminosity* $\mathcal{L}_{\mathcal{M}}$, the highest energies of accelerated particles are achieved in transrelativistic MHD flows with $\beta_{\rm f} \lesssim 1$. Such flows can be realized in some classes of supernovae [50] and in fast transient sources [51]. It follows from estimate (2) that only sources with a power per unit solid angle of $\sim 10^{36}$ erg s^{-1} or higher can be accelerators of particles in the PeV range or above. Possible models of above-PeV CR acceleration in galactic sources are associated with supernovae and with relativistic objects (magnetized neutron stars and accreting black holes) produced during the collapse of massive stars. The issue comes down to studies of CR acceleration mechanisms and to observations of nonthermal radiation of sources up to photon and neutrino energies of the order of a PeV, which we will discuss further after a brief review of the results of supernova observations related to the issue of particle acceleration. The search for cosmic particle accelerators and studies of probable CR sources are conducted by orbital X-ray and gamma-ray telescopes, as well as by the modern ground-based atmospheric Cherenkov observatories the Large High Altitude Air Shower Observatory (LHAASO) [52] and Taiga [21]. In Sections 6 and 7, we discuss some new results of X-ray and gamma-ray observations of supernova remnants. The first results of observations of high-energy astrophysical neutrinos [53] demonstrate the prospects for searching for CR accelerators.

3. Supernovae and their remnants

Theoretical models predict a supernova explosion as the final evolution phase of stars with masses $\gtrsim 8 M_\odot$ and accreting white dwarfs in binary systems. About a hundred years ago, a start was made on the study and classification of observed extragalactic supernovae explosions. The spectroscopic classification of supernovae (SNs) has historically been based on the absence (in type I explosions) or presence (in type II explosions) of hydrogen lines in the phase of highest brightness. Spectral lines in many cases have a PCygni-type profile with a Doppler shift to the blue side of the absorption lines and with a broadening of the emission lines corresponding to ejecta expansion velocities of $\sim 0.03\,c$ [54–56]. In type I SN explosions, several subtypes are distinguished: Ia, Ib, and Ic,

of which Ia supernovae make up a significant part. Such supernovae lack hydrogen lines and have strong absorption lines of singly ionized silicon (Si II). In type Ib supernovae, strong neutral helium lines and weak (or completely absent) silicon lines are visible at peak brightness. Finally, type Ic supernovae lack strong lines of both silicon and helium, but often show strong absorption in the neutral oxygen line. Observations of the light curves of SNe — the dependence of their luminosity on time (either the total in the UV, optical, and IR ranges (UVOIR), or bolometric) — demonstrate significant differences among supernovae of type Ia, Ib/c, and II. The diversity of SN types reflects the different physical nature of these objects and the circumstellar environment produced by the evolution of the progenitor star. Type Ia SN outbursts do not leave a compact remnant, dispersing all the matter of the progenitor star into the external environment. Type II and Ib/c SN outbursts are accompanied by the collapse of the core of the progenitor star and leave behind a compact remnant.

The vast majority of type Ia supernovae have highly uniform light curves. They typically reach a peak brightness with a UVOIR luminosity of $\sim 3 \times 10^{43}$ erg s^{-1} approximately three weeks after the outburst. The luminosity then drops at characteristic decay times of the radioactive isotopes ^{56}Ni and ^{56}Co. Over the course of several months, a typical Ia supernova emits energy of the order of 10^{49} erg. This is about one percent of the kinetic energy of the matter ejected by the supernova into the circumstellar medium. Observations of type Ia supernovae are of fundamental importance for determining the parameters of the cosmological model. The progenitors of Ia SNs are massive white dwarfs formed either by accretion of matter from a companion star or by the merger of two low-mass white dwarfs.

As for II and Ib/Ic supernovae, their light curves are quite diverse. Their shape and luminosity at peak brightness depend on a number of factors: on the energy release of the compact remnant, on the interaction of the supernova ejecta with the circumstellar medium (formed during the mass loss phase of the presupernova), and on the influence of the companion star (if the progenitor star of the supernova was part of a binary system) [57]. The light curves of Ib/Ic supernovae are often similar to those of Ia, but their luminosities at maximum brightness are usually appreciably lower. The progenitors of Ib/c are massive stars that presumably lost their hydrogen envelope completely at the presupernova stage. Type II supernovae are also divided into subtypes: IIP, IIL, IIb, etc., which differ in their light curve profiles and spectra. The progenitors of IIP supernovae are considered to be red supergiants that have retained most of their hydrogen envelope. In IIL/IIb supernovae, the progenitors were able to retain only a small part of the hydrogen envelope. Another possible subtype of supernovae (represented by SN 1987A) have blue supergiants with a massive envelope as progenitors. Rarely (with a frequency of $\lesssim 10^{-3}$ of the frequency of typical SNs), the interaction of the supernova ejecta with the circumstellar environment can (under certain conditions) give rise to especially bright (superluminous) supernovae with a luminosity tens of times higher than typical [58].

Observations with large optical telescopes make it possible to detect weak linear polarization of radiation at a level of about one percent. It is interesting that the degree of polarization of type Ia SNs rises with time up to the peak brightness and then decreases. For SNs of all other types, the temporal behavior of the degree of polarization is the opposite. The interpretation of these data comes down to the fact that in Ia SNs the asymmetric distribution of the radiating ejecta at the initial moments is replaced (after the peak brightness) by an expansion mode close to spherically symmetric. The sequence is reversed for some Ib/c and SN II SNs, which indicates an asymmetry in the expansion of the main mass of the ejecta after the peak brightness. X-ray observations of young supernova remnants also, in a number of cases, demonstrate the presence of asymmetry in the expansion of the ejecta and the distribution of the initial velocities of neutron stars associated with such asymmetry (so-called natal kicks) [59].

It is extremely rare to identify the probable progenitor star of an SN (as was the case with 1987A SN). Much more often, it is possible to determine the type of galaxy which the SN outburst occurred in and even localize the position of this SN in the galaxy. In elliptical galaxies with an old population of stars, only Ia SNs are found. As for SNs of types II and I/c, they are always observed in spiral and irregular galaxies and, as a rule, in spiral arms and star-forming regions.

Models of the origin of Ia SNs assume that their progenitors are degenerate stars: white dwarfs consisting mainly of carbon, oxygen, and silicon. The stability of white dwarfs is maintained by the pressure of the degenerate electron gas. If the mass of the dwarf exceeds the Chandrasekhar limit (about $1.4\,M_\odot$), it loses hydrostatic stability and its subsequent gravitational compression launches a wave of deflagration thermonuclear burning outward from the center of the star. This burning is accompanied by the production of radioactive elements of the iron group, ^{56}Ni and ^{56}Co, the whose decay subsequently forms the characteristic light curve of Ia SNs. There are several scenarios leading to a dwarf gaining mass above the Chandrasekhar limit. The main ones are considered to be the merger of two white dwarfs and the accretion of matter from a companion star in a binary system by a white dwarf. As a result of the outburst of a Ia SN, a stellar remnant is not produced; all products of thermonuclear burning are ejected into the environment with a typical kinetic energy of $\sim 10^{51}$ erg, which gives initial velocities of the shock wave of the SN shell of $\sim 10{,}000$ km s^{-1}.

The mechanism of Ib/c SN and II SN production is caused by the collapse of the cores of massive stars with mass $\gtrsim 8\,M_\odot$, belonging to a young population of stars with ages $\lesssim 30$ million years (while the progenitors of Ia SNs belong to an old population with an age of more than a billion years). From the idea of Baade and Zwicky [60] about gravitational collapse as a source of SN energy, there follows an estimate of the energy $E_{\rm SN}$ released during the collapse of the stellar core into a protoneutron star with mass $M_{\rm pns}$ and radius $R_{\rm pns}$:

$$E_{\rm SN} \sim \frac{3GM_{\rm pns}^2}{5R_{\rm pns}} \sim 3 \times 10^{53} \ \ \text{erg},$$

where the numerical value was obtained for $M_{\rm pns} = M_\odot$ and $R_{\rm pns} = 12$ km. The main part of this energy after the production of a hot protoneutron star in 10–20 s is carried away by neutrinos with an energy spectrum in the MeV range. Neutrino emission was detected from SN 1987A in the Large Magellanic Cloud [61]. Observations of this supernova provide very interesting information about the physics of SNs. The detection of 19 neutrinos emitted by SN 1987A over a time interval of about 13 s has been the only one to

date. Modern neutrino observatories have significantly better sensitivity, and neutrino emission models predict the expected properties of the neutrino signal for various types of collapsed SNs [62, 63].

The collapse of massive stars is accompanied by powerful and nonuniform heating of the stellar matter by neutrino flows in the first minute after the bounce of the collapsed core. Such heating induces strong turbulence behind the shock wave accompanying the bounce. For several hundred milliseconds, the inner layers of the progenitor star can undergo powerfull accretion onto this shock [64]. This can cause the shock to stall or even retreat, since it spends most of its energy on counteracting the dynamic pressure of the accreting matter and on the photodissociation of its partially preserved atomic nuclei.

Simultaneous modeling of neutrino transport and turbulence anisotropy is crucial for solving the problem of relaunching the outward propagation of the shock. It is this shock that is called to throw off most of the progenitor material into the interstellar medium and to provide, upon reaching the stellar surface, a SN event with a typical kinetic energy of ejecta of $\sim 10^{51}$ erg.

Realistic simulations of the turbulence effects and the observed high proper velocities of neutron stars call for three-dimensional collapse simulations and computers with petaflop-level performance. Despite the significant difference between the production mechanisms of type Ia thermonuclear supernovae and the above-described core collapse of a massive star, the kinetic energies of the ejecta in both cases for most typical SNs are $\sim 10^{51}$ erg. However, there are rare supernovae with observed manifestations that differ greatly from the majority. For example, observations of the type IIn 2016aps SN (this type is distinguished by the presence of narrow hydrogen lines in the spectrum) showed a high luminosity of $\sim 4.3 \times 10^{44}$ erg s^{-1} and the time-integrated energy of the observed radiation of $(5.0 \pm 0.1) \times 10^{51}$ erg [65]. Such a high value of the released energy would require almost complete thermalization of the kinetic energy of a typical supernova in a short time. The authors of the observations suggest that this powerful SN had a kinetic energy exceeding 10^{52} erg and had a massive circumstellar envelope ejected by the progenitor before the collapse of its core. Possible models of the 2016aps SN included the formation of a millisecond magnetar or, alternatively, the explosion of a so-called *pair-instability* SN, in which, during the collapse of a massive helium core with a mass of $\sim$ (64–84) $M_\odot$, hydrodynamic instability develops due to an avalanche-like conversion of photons into electron-positron pairs. The expected frequency of neither scenario exceeds 10^{-3} of the frequency of collapsing SNs, the expected frequency of events with a magnetar being significantly lower.

Estimates of the frequency of supernova explosions in the Galaxy currently have very significant uncertainties. The authors of study [66] estimated the frequency of collapsed SNs as $3.2^{+7.3}_{-2.6}$ per century, and the frequency of thermonuclear Ia SNs as $1.4^{+1.4}_{-0.8}$ per century. At the same time, the total frequency of SNs is $4.6^{+7.4}_{-2.7}$ per century, which corresponds to a star formation rate in the Galaxy of $3.8^{+8.3}_{-3.0}\, M_\odot$ year^{-1}. The authors of study [67] recently obtained noticeably lower estimates of the frequency of collapsed SNs (0.4–0.5 per century) and the star formation rate of SNs in the Galaxy ($0.67^{+0.09}_{-0.01} M_\odot$ year^{-1}). For the near vicinity of Earth, their estimate gave 2.5 collapsed SNs per billion years. With a SN frequency in the Galaxy of the order of one event per hundred years and a typical kinetic SN energy of 10^{51} erg, their power exceed 10^{41} erg s^{-1}. This is sufficient, in the theory of V.L. Ginzburg and S.I. Syrovatskii, to maintain a quasi-stationary distribution of CRs in the Galaxy with a large halo, provided a $\sim 10\%$ efficiency of acceleration processes of CRs with energies in the GeV–TeV range. The frequency and spatial distribution of SNs in the Galaxy are significant factors in the chemical evolution of galaxies, CR acceleration, and the formation of interstellar magnetic fields [69] and interstellar turbulence [68].

Estimates of the SN frequency from observations of radio emission from supernova remnants in the local group of galaxies are based on models of remnant evolution and particle acceleration under different conditions of the surrounding interstellar medium [70]. Of particular interest are high-latitude SN remnants, such as G70.0-21.5, an extended remnant (probably a Ia SN), identified by optical filaments and a high-velocity white dwarf, a possible companion of an exploded star [71]. The all-sky X-ray survey by the Spectrum Roentgen-Gamma Observatory [72] revealed several new supernova remnants, including the high-latitude SRGe J0023 + 3625 (or, according to another nomenclature, G116.6-26.1) [73]. The age of the G116.6-26.1 remnant estimated on the basis of X-ray data is about 40,000 years, and the weak radio emission observed from it is compatible with the hypothesis of adiabatic compression of CRs and the magnetic field of the galactic halo (the van der Laan model [74]), applicable to fairly old remnants of SNs of the Cygnus Loop type [75]). This allows the use of evolved high-latitude SN remnants to study magnetic fields and relativistic particles in the galactic halo.

More frequent than supernovae are thermonuclear outbursts on the surface of accreting white dwarfs in close binary systems, representing novae [76]. The frequency of novae in the Galaxy is estimated at 50^{+31}_{-23} events per year [77], and the energy of a flare usually does not exceed 10^{47} erg. Gamma radiation detected from a flare of the famous repeating nova RS Ophiuchi (which flares periodically once every few decades) proved the presence of the effect of acceleration of relativistic particles [78]. However, an analysis of the possible contribution of novae, performed in Ref. [79], led to the conclusion that they make a relatively insignificant contribution to the global effect of acceleration of galactic CRs, although, in the vicinity of the order of a parsec from the source, nova flares can enhance local CR flows.

Acceleration and confinement of ultra-high-energy CRs in the Galaxy does not seem possible. However, the origin of CRs with energies up to 1000 PeV is an open question. It is important to understand which galactic sources can accelerate protons above a PeV. Rare powerful SNs (like SN 2016aps) can, in principle, be sources of CRs with energies above a PeV in the spectrum knee region, as well as sources of high-energy neutrinos [80–83]. The anomalously high luminosity of rare SNs like SN 2016aps and the emitted energy of more than 10^{51} erg over a period of about a year suggest an effective interaction of the ejecta with a massive circumstellar envelope. There are observational indications of the production of a dense massive circumstellar envelope by the wind of a red supergiant immediately before the core collapse [84, 85]. Acceleration of particles by such SNs can be expected at the initial stage of the evolution of an SN remnant, in the region of intense interaction of the shock wave with the dense shell.

Multichannel observations of the 2023ixf type II supernova from a collapsed red supergiant in the nearby galaxy M 101 at a distance of 6.85 Mpc were performed in Ref. [86]. The authors' goal was to estimate the CR acceleration efficiency in the first few days after the collapse. Estimates of the mass loss rate of the giant star in the years before the collapse yielded a value of $\sim 10^{-2}\, M_\odot\, \mathrm{year}^{-1}$, and estimates of the power released by the shock wave during its passage through the dense shell yielded a value of $\gtrsim 5 \times 10^{40}$ erg s^{-1} [87]. Based on the upper limit on the emission of photons with energies above 100 MeV (obtained by the Fermi Gamma-ray Observatory) and using a simplified spherically symmetric model of the circumstellar medium, the authors of the work established an upper limit of about 1% on the CR acceleration efficiency in the first month of SN 2023ixf evolution. It is suggested that this limit may be loosened to $\sim 10\%$ in a more complex model of the SN interaction with the ejected envelope of a pre-supernova [86]. Unfortunately, the chance to observe gamma-ray photons with energies above 100 TeV with ground-based Cherenkov telescopes, which could directly confirm the acceleration of PeV-energy protons, is limited to distances of the order of a Mpc. Even for the nearby SN 2023ixf, the absorption of photons with energies $\gtrsim 100$ TeV due to interaction with relic photons greatly reduces the flux, so observations are limited to lower energies. Unlike photons, high-energy neutrinos from such supernovae are not subject to absorption. The emission of neutrinos with energies above 10 TeV during interaction with dense shells of the circumstellar medium of a strong shock wave (SW), which, after emerging on the stellar surface of a collapsed star, transitions from a radiation-dominated phase to a collisionless phase might explain the observed diffuse neutrino fluxes [88].

Sources of long gamma-ray bursts are associated with rare types of supernovae (mainly Ib and Ic), which produce relativistic plasma outflows with a Lorentz factor $\gtrsim 100$ [89]. Such bursts occur approximately 1% as frequently as the outbursts of collapsing supernovae (in particular, type Ib/c SNs). SNs with moderately relativistic ejecta velocities of $\sim 0.8\, c$ are also observed [90–93]; they make up an intermediate class of SNs located between relativistic sources of gamma-ray bursts and the main population of SNs with nonrelativistic ejecta velocities. In relativistic SNs, the ejecta with a mass of $\sim 10^{-5}\, M_\odot$ moves with initial velocities of $\gtrsim 0.3$–$0.8\, c$. A possible mechanism for the formation of SNs with a relativistic ejecta may be associated with the activity of a millisecond magnetar as a central source [92]. The frequency of occurrence of a transrelativistic SN is still very uncertain and probably does not exceed 1% of the frequency of ordinary SNs, and the kinetic energies of such supernovae are $\sim 10^{49}$ erg. Transrelativistic SNs can accelerate CRs to energies above a PeV [94–97]. Recently discovered fast optical transient sources with moderately relativistic velocities can also be CR accelerators to energies significantly above a PeV [51, 98]. Observations of supernova remnants and processes in the solar wind show that particle acceleration in supersonic flows occurs via shock waves, so we will discuss the features of supernova shock waves.

4. Shock waves in supernova remnants

The collapse of the core of a massive star is accompanied by the production of a shock wave that propagates through the layers of the star that are external to the core and emerges on its surface. At the moment of emergence on the surface, the wave is radiation-dominated. The main fraction of the kinetic energy of upstream flow is transformed at the shock front into radiation pressure in the downstream flow. The optical thickness in a radiation-dominated shock wave should exceed c/u_{sh}, where u_{sh} is the shock wave velocity. The dominance of radiation pressure over the gas pressure of plasma particles behind the shock wave front suggests that the shock wave velocity and the plasma density in the shock upstream satisfy the relation

$$u_{\mathrm{sh}} > 2 \times 10^{-4}\, c \left(\frac{n}{10^{15}\ \mathrm{cm}^{-3}} \right)^{1/6}.$$

As the nonrelativistic shock wave propagates, the optical thickness arising from Thomson scattering falls below c/u_{sh}. Then, the shock wave leaves the radiation-dominated stage and becomes a plasma shock wave. In a relativistic shock wave, the above condition is violated by the production of $\mathrm{e}^{\pm}$ pairs and the Klein–Nishina effect [99]. Furthermore, the dissipation of kinetic energy in the shock wave is due to plasma mechanisms. With a drop in plasma density after breaking through the stellar surface, the shock wave passes into the mode of a collisionless shock wave.

In a collisionless shock wave, the structure of the viscous jump, where the super-Alfven flow slows down and the plasma heats up, is determined by the development of plasma instabilities[2] [100, 101]. Shock waves in stellar winds, in supernova remnants, and in many other sources of energetic particles and nonthermal radiation are collisionless. The width of the front of a strong collisionless shock wave (the size of the dissipation region) in a rarefied plasma outside a star is many orders of magnitude smaller than the Coulomb path of particles in a rarefied plasma [22, 103–106]. We will further consider so-called supercritical shock waves, the structure of which is determined by plasma instabilities produced by ions reflected into the region in front of the viscous jump [22, 101, 103].

The structure of the front of a collisionless shock wave depends on its velocity, composition (ions–electrons or $\mathrm{e}^{\pm}$ pairs) and degree of plasma magnetization, and the direction of the magnetic field relative to the normal to the shock wave front. A detailed analysis of the role of different plasma instabilities in the formation of shock waves can be found in Ref. [106]. In a rarefied electron–ion plasma, the width of the shock wave is characterized by the inertial length of ions l_{i} instead of the Coulomb mean free path, and in a rarefied electron-positron plasma, by the inertial length of electrons l_{e}:

$$l_{\mathrm{e,i}} = \frac{c}{\omega_{\mathrm{pi,pe}}} = \sqrt{\frac{m_{\mathrm{i,e}} c^2}{4\pi n_{\mathrm{i,e}} e^2}}. \tag{3}$$

Here, ω_{pi} and ω_{pe} are the ion and electron plasma frequencies, respectively. The inertial length of an ion in an electron-proton plasma is $l_{\mathrm{i}} \approx 2 \times 10^7\, n_{\mathrm{i}}^{-1/2}$ [cm], where the ion density n_{i} in the proper flow frame of reference is expressed in cm^{-3}. The Coulomb range of a proton (and electron) relative to scattering in an equilibrium plasma with temperature T_{eV}, expressed in eV, is approximately $3 \times 10^{12}\, T_{\mathrm{eV}}^2/n_{\mathrm{i}}$ [cm].

[2] A very interesting history of the beginning of the study of collisionless shock waves physics can be read in the book by R.Z. Sagdeev [102], a direct participant and one of the pioneers in their discovery and research.

The nature of the mechanisms of scattering of particles of incoming plasma flow by electromagnetic field fluctuations and, in particular, the mechanisms of particle heating in the absence of Coulomb collisions make it possible (and inevitable in a broad region of the parameter space of the shock wave) to form a substantially nonthermal particle distribution. Nonthermal energetic particles can escape into the prefront of the shock wave and influence the flow of the incoming plasma, so that they are an integral part of the large-scale structure of the collisionless shock wave.

4.1 Structure of collisionless shock waves

Modeling the structure of a collisionless shock wave is a nonlinear kinetic problem with strong coupling of substantially different spatial scales. Complete consistent kinetic models require computer resources that are currently unavailable. However, a number of important results concerning the processes of viscous jump formation and particle injection into a nonthermal distribution can be obtained using plasma modeling of shock wave production by *particle-in-cell* (PIC) methods [107–109]. *Particle-in-cell* (PIC) methods are based on the representation of real particles by macroscopic particles with an extended charge distribution. The trajectories of the macroparticles are calculated from the values of the electromagnetic fields on the Eulerian grid. The field values themselves, in turn, are calculated from the positions and velocities of the macroparticles. The plasma parameters corresponding to the conditions of SW propagation in circumstellar and interstellar media yield a value of the Debye radius much shorter than the value of the electron inertial length l_e. This determines the depth of penetration of low-frequency electromagnetic radiation into the plasma. In turn, the ion inertial length is much shorter than the ion transport path length relative to the Coulomb scattering estimated above. Standard schemes of PIC methods calculate the electromagnetic field sources at each stage of the iteration procedure based on the current position and velocity of each macroparticle. The resultant charge densities and currents allow one to calculate the values of the electric and magnetic field strengths by solving Maxwell's equations. The field strengths, in turn, allow calculating the Lorentz force acting on each macroparticle, and thereby calculating new values of the positions and velocities of the macroparticles. Iterations of this scheme are subsequently performed [107–109]. The construction of stable PIC models involves solving a number of complex problems associated with the introduction of distributed charges and currents, with the choice of the number of macroparticles per cell, with the reduction of noise effects, and with the elimination of nonphysical Cherenkov instability. The dimensionality of the model space is essential for calculating the motion of particles in electromagnetic fields, since ignoring at least one coordinate limits the motion of particles across the magnetic field [110]. Calculations of the structure of relativistic shock waves in the electron-positron plasma of pulsar winds differ significantly from those of nonrelativistic shock waves typical of supernova remnants. In the former case, the width of the viscous shock wave jump is determined by the skin layer thickness l_e, while the characteristic widths of nonrelativistic shock waves of supernovae are tens and hundreds of inertial lengths of the ion l_i. The significant difference between the electron and ion inertial lengths in electron-proton plasma, as well as the need to have a computational domain of hundreds of inertial lengths, makes it expensive to simultaneously take these two components into account at the level of macroparticles. Therefore, a resolution of 1024^3 (or a similar resolution, but stretched along the flow direction and compressed along other axes) is insufficient to perform 3D modeling of nonrelativistic shock waves in electron-proton plasma using PIC models. In contrast, models of relativistic waves with large Lorentz factors of the flow made it possible to study the structure of such waves and demonstrated the effect of forming stable nonthermal distributions of accelerated particles [111–113]. Calculations of the structure of the front, as well as the injection and acceleration of electrons and ions for shock waves with subrelativistic velocities of $\sim (0.2\text{–}0.8)\,c$, performed in Refs [51, 114–116], correspond to the conditions in relativistic supernovae with a small ejecta mass and a (probable) central source (magnetar) [50, 90, 117]. Subrelativistic shock waves are also formed in anisotropic outflows of microquasars with a supercritical accretion rate [118, 119].

Modeling of the structure of nonrelativistic SWs with velocities $\lesssim 0.03\,c$, realized in the majority of supernova remnants with ejecta mass $\gtrsim M_\odot$, in some cases can be successfully performed using a simplified version of PIC: the so-called hybrid codes (see, for example, Refs [105, 108, 120–122]). In hybrid versions of PIC, ions are considered as model macroparticles, while the electrons are considered as a massless neutralizing fluid. In the equations for the electromagnetic field, the displacement current is ignored, and therefore the electric field is calculated from the generalized Ohm's law, i.e., from the condition of equality of the volume electric force (acting on the massless electron fluid) to the set of other forces in the Euler equation for electrons, which are caused by the moments of ion distribution and include pressure gradients, the Ampere force, and viscous stresses. The absence of a displacement current in the model limits its application to nonrelativistic flows. As a rule, in hybrid modeling of a collisionless shock wave in supernova remnants interacting with circumstellar matter within the width of its front (several ten ion inertial lengths l_i), the charge states of ions can be considered unchanged for plasma with an ion density $\lesssim 10^{10}$ cm^{-3}. Hybrid models allow calculating the shock wave structure on spatial scales greater than $10{,}000\,l_i$. Under conditions of limited resolution, this allows successfully constructing models of nonrelativistic supercritical shock waves.

The simulation of a collisionless shock wave begins with the initialization of the corresponding plasma flow. In the PIC method, the shock wave can be initiated by a collision of two flows (or plasma clouds) moving towards each other and having a magnetic field directed along the velocity of their motion (see, for example, Ref. [106]). A common method for initializing a shock wave is to reflect a supersonic and super-Alfven particle flow from a conducting stationary wall. Particles of the supersonic flow with a Maxwellian distribution are injected at the opposite boundary at the end of the simulation domain, where the open boundary is located. Periodic boundary conditions are specified along the spatial coordinates transverse to the flow direction. After the flow is reflected, a collisionless shock wave front is formed, moving away from the wall in the positive direction of the spatial axis directed against the flow. A brief description of the method for hybrid simulation of shock waves in a multicomponent electron-ion plasma is given in Ref. [93], where Figs 2–4 show the results of modeling the structure of the ion phase space for a strong shock wave with different inclination angles of a

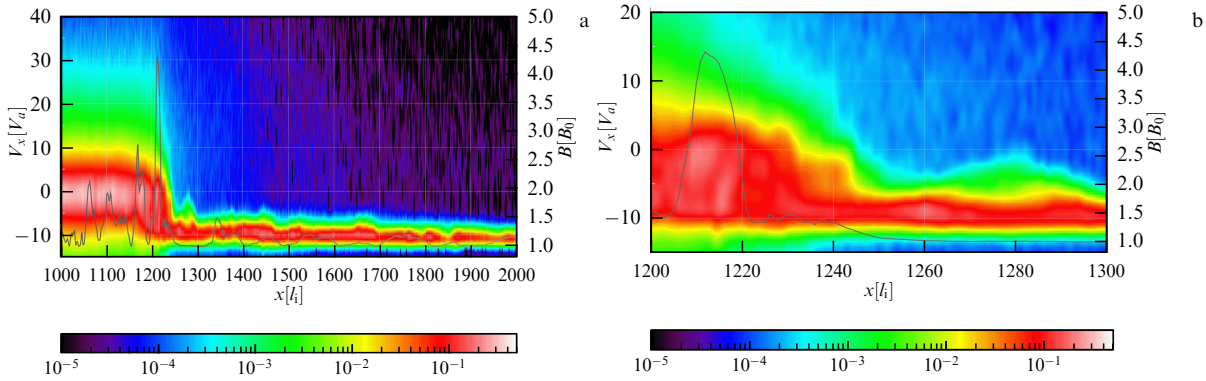

Figure 4. Structure of the V_x–x phase space of particles for a quasi-longitudinal shock wave with an angle between the magnetic field and the normal to the front of 10°, Alfven Mach number $M_a = 10$, and a ratio of the plasma pressure to the magnetic pressure in the incoming flow equal to 0.1. Calculations are performed using a hybrid code [123], in the flat (2D) geometry. The simulation domain includes 10,000 × 600 × 1 square cells with an edge length equal to the ion inertial length (l_i). The black solid line depicts the smoothed profile of the magnetic field.

uniform magnetic field to the normal of the shock wave, which were obtained using the hybrid PIC code Maximus [123].

An important feature of quasi-longitudinal shock waves is the formation of a *precursor*. This is the name given to the region ahead of the wave front disturbed by reflected and accelerated particles. This region is shown in Fig. 4a. The population of reflected particles with a positive velocity is visible to the right of the magnetic field peak, which is plotted on the phase plane as a line for convenience. Analysis of the trajectories of the reflected particles suggests that these particles are not simply mirror-reflected from the front, but move along it for some time and gradually gain energy. In the laboratory frame of reference associated with a stationary reflecting wall, some of the ions acquire velocities in excess of +2.5 Alfven velocity, which allows them to move away from the shock front upward along the supersonic flow incident on the front. The shock front itself may be associated with the magnetic field peak, indicated by a solid line in V_x–x phase planes. In Figure 4b, the shock front region is shown on an enlarged scale. For particles with positive velocities penetrating into the incoming flow, velocity blurring and the formation of a diffuse ion population are noticeable. Due to the absence of Coulomb relaxation, fast ions of such a population will be injected into the Fermi acceleration mechanism on a shock wave, which we will consider in Section 5. Electron injection is a much more complex process due to the large difference between the gyroradii of ions and electrons. The structure of supercritical shock waves, which are most interesting as effective particle accelerators, is determined by processes on the ion scale, since in fast SWs the flow energy is concentrated precisely in the ions. To be injected into acceleration, electrons must first reach energies corresponding to the equality of their Larmor radii with those of ions. Electrons can do this due to interaction with turbulent fluctuations formed by ion flow instabilities [124]. Note that PIC modeling requires lengthy simulation to take into account the electron dynamics. Such a 1D simulation performed in [125] suggested that, in a quasi-parallel shock wave, the electrons are initially preheated during their drift motion, and then they are pre-accelerated during the interaction with the Bell modes in the shock wave pre-front. The authors of the indicated work estimated the electron-to-ion number ratio at $\lesssim 10^{-2}$ among the particles injected into acceleration in a strong nonrelativistic wave.

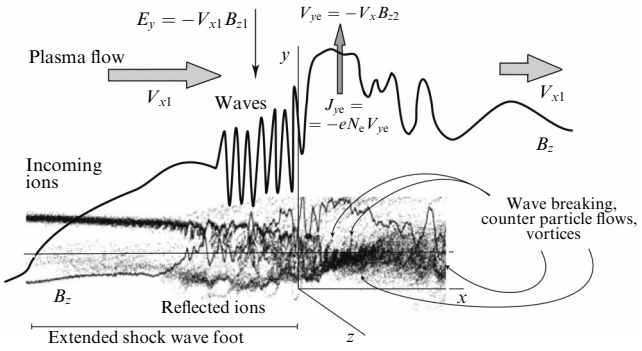

Figure 5. Schematic structure of a collisionless supercritical quasi-transverse shock wave. Shown are the magnetic field and density profiles of the plasma in the region of the dissipative viscous jump caused by ion reflections. The magnetic field of the current associated with the reflected ions forms (in front of the viscous jump) a magnetic field structure, called the shock wave foot. The electric field directed along the shock wave front is capable of accelerating particles via the electric drift mechanism. (Reproduced from Ref. [22]; see also Refs [103, 104].)

Simulations based on different versions of the PIC method have shown that the width of quasi-longitudinal SWs amounts to $\gtrsim 100\, l_i$, while that of quasi-transverse shock waves amounts to $\sim 10\, l_i$. The structure of a collisionless quasi-transverse shock wave is illustrated in Fig. 5, which shows the characteristic features of the formation of the front of such a wave (for more details, see Refs [22, 103, 104]). Models of quasi-transverse shock waves show that electrons can be effectively injected into the Fermi acceleration mechanism. At the same time, the presence of a diffuse population of ions escaping upstream is often not pronounced. Analysis of the PIC model combined with the MHD description of large scales shows that, for each angle of inclination of the field to the normal to the shock wave front, there is a critical Alfven Mach number M_a, starting from which the mechanism of diffusive acceleration of particles is triggered [126]. For example, for a field tilt angle of 60°, this number should exceed 46. For $M_a > 50$, the injection and acceleration of ions hardly depend on the plasma magnetization level. It should be borne in mind that PIC models, as a rule, fix the magnetic field direction in the unperturbed incoming plasma flow ahead of the shock wave. Observations of young SN remnants testify to the formation of a spectrum of accelerated protons in strong supernova SWs that lasts for more than 8 decades. The

dynamic range of magnetic turbulence generated by accelerated particles has a similar extent. Since there is a strong coupling between plasma microscales (determining injection) and long-wave fluctuations (generated by accelerated particles), the above-mentioned fixation of the field direction at the boundary of the simulation domain, which is much narrower than the region of turbulence generation by accelerated particles, limits the applicability of combined PIC-MHD models. In strong extended SWs of supernova remnants, accelerated ions and electrons acquire relativistic energies and produce nonthermal radiation from these remnants, which is observable from radio waves to gamma rays. High-energy particles leaving the accelerator replenish the population of cosmic rays in the Galaxy.

5. Cosmic ray acceleration mechanisms

The main sources of plasma flow energy in CR accelerators are related to the gravitational collapse of stars, with accretion onto compact objects, thermonuclear flares, and the braking of rapidly rotating relativistic stars. CR accelerators in the Galaxy should provide the conversion of the power of highly conductive plasma flows to relativistic particles with an efficiency of about 10% or higher. This indicates the probable importance of including the nonlinear feedback effects of accelerated relativistic particles on background plasma flows and magnetic fields. The energetic ejecta of a supernova propagates with an initial velocity of several thousand km s^{-1} and produces strong shock waves, first in the circumstellar medium and then in the interstellar medium.

In systems with high magnetization, the source of energy for accelerated particles is the dissipation of magnetic fields in current layers of highly magnetized plasma [138–142]. Such mechanisms are typical of stellar flares (including solar ones), the magnetospheres of Earth and the planets, and flares of magnetars. The slowing-down of rapidly rotating pulsars produces relativistic winds of electron-positron pairs with high initial magnetization $\sigma \gg 1$ outside the region of their light cylinder. The conversion of the energy of such a wind into accelerated particles suggests the presence of reconnection of magnetic field lines with the production of electric fields [143, 144].

High-velocity flows of supernova ejecta with shock waves have Alfven Mach number $M_a \gg 1$ and, accordingly, magnetization parameter $\sigma = 1/M_a^2 \ll 1$. The particle acceleration mechanism proposed by Fermi [18] works effectively in flows of weakly and moderately magnetized plasma. We will dwell on the features of the Fermi mechanism in more detail, since it allows the shock wave to effectively accelerate particles and produces extended power-law energy spectra of nonthermal accelerated particles similar to those observed. In addition, modeling of the Fermi acceleration process has opened several important approaches to the problem of the relationship between regular and stochastic particle dynamics and to the problem of nonlinear dynamics of collisionless shock waves in cosmic plasma.

5.1 Fermi acceleration

In the original version of the Fermi mechanism, high-energy charged particles of cosmic rays are treated as test particles that interact with the magnetic and inductive electric fields of the background plasma motion and experience ionization energy losses due to Coulomb collisions in the plasma.

When a fast particle with velocity βc, energy E, and pitch angle θ is reflected from a magnetic cloud of background plasma moving with velocity $\tilde{\beta}c$ relative to the laboratory frame of reference, the change in particle energy E' will be [18]

$$\frac{E'}{E} = \frac{1 + 2\tilde{\beta}\beta\cos\theta + \tilde{\beta}^2}{1 - \tilde{\beta}^2}\,. \tag{4}$$

Since the probability of head-on collisions is higher than the probability of overtaking collisions, in multiple scatterings of a fast particle by inhomogeneities with random velocities, the resulting effect is reduced to the gain in energy by the particle after averaging over the ensemble of scatterers [18]:

$$\left\langle \ln\left(\frac{E'}{E}\right)\right\rangle = 4\tilde{\beta}^2 - 2\tilde{\beta}^2\beta^2\cos^2\theta\,. \tag{5}$$

Fermi noted that stochastic acceleration in the interstellar medium should be slow enough due to the low velocities of scatterers ($\tilde{\beta} \ll 1$), and the rate of energy gain by heavy nuclei cannot effectively compete with the Coulomb ionization energy losses of highly charged ions with energies below GeV. So, stochastic acceleration requires an effective injection mechanism, i.e., preliminary acceleration of particles to an energy starting from which the Fermi acceleration rate exceeds the loss rate. In a subsequent paper [145], Fermi suggested that stellar processes are the injectors of fast particles in the acceleration mechanism. He also noted the role of the diffusion outflow of cosmic rays from the Galaxy with a characteristic time of about 10 million years and pointed out the potential importance of magnetic field jumps at shock wave fronts for a significantly more efficient scattering of high-energy charged particles. Several years after Fermi's work, the solar wind and collisionless shock waves in cosmic plasma, which we discuss in Section 4, were discovered. The mechanism of cosmic ray acceleration due to interaction with magnetic inhomogeneities, proposed by Fermi [18, 145], turned out to be universal and very effective, and it underlies the processes of particle acceleration by plasma flows with different configurations and degrees of magnetization (see, for example, Refs [141, 146–148]).

An attempt by S. Ulam to study the Fermi mechanism using the simplest numerical one-dimensional mathematical model constructed to observe the evolution of the energy of a particle moving between ideally reflecting walls oscillating according to a given regular law initially resulted in the absence of growth in the average particle energy with time [149], i.e., in the absence of acceleration. A subsequent detailed analysis of the Ulam model with regular motion of the reflecting walls in the work of G.M. Zaslavskii and B.V. Chirikov [150] revealed the boundaries of the region of particle velocities separating completely stochastic behavior with the presence of Fermi acceleration at low particle velocities $v \lesssim V\sqrt{L/a}$ from the region of high particle velocities, where this velocity experiences only stable small oscillations. Here, V is the amplitude of the wall velocity, and L and a are the distance between the walls and the amplitude of the wall displacement, respectively. Between the stochastic and regular regimes there is an intermediate region, which communicates with the stochastic regions of the phase space. For $\sqrt{L/a} \gg 1$, in this model, the Fermi acceleration effect is clearly expressed in the stochastic region, and it can be described by Fokker–Planck-type equations [150]. The study of the simplified Fermi acceleration model initiated an interesting development of the theory of stochastic instabil-

ity of nonlinear oscillations [151–153], which is essential for understanding the connections between regular particle dynamics and statistical mechanics.

An effective scenario of high energy particle acceleration by nonrelativistic shocks was proposed in 1977, which involved a regular change in the particle energy according to Eqn (1) but with multiple returns of some particles to the shock compression region [154–157]. Particle scattering by magnetic inhomogeneities both in the shock upstream and downstream flows result in the multiple return to the SW front providing highly super-adiabatic particle acceleration. Indeed, particle scattering in the frame of reference associated with a uniform flow both upstream and downstream of the shock does not change the particle energy. A change in the magnitude of the particle momentum δp occurs only when crossing the SW front. In one cycle of front crossing, including one head-on collision with a scatterer in the incoming flow and one collision in the outgoing flow, the change in the magnitude of the momentum averaged over the close-to-isotropic particle velocity distribution in the rest frame of the shock wave front is

$$\frac{\delta p}{p} = \frac{4(u_1 - u_2)}{3v} .$$

The approximate isotropy of the particle momentum distribution is due to the large number of collisions and nonrelativistic velocities of the nonuniform flows. Here, u_1 is the velocity of scatterers in the shock upstream flow, and u_2 is their velocity in the shock downstream (both measured relative to the SW front at rest). For an infinite medium, with any finite scattering probability, a particle will return to the SW front from the shock upstream with unit probability. The probability of returning to the SW front from the shock downstream in the case of scattering of a fast particle $v \gg u_2$ is approximately equal to $(1 - 4u_2/v)$. In an idealized plane SW in an infinite medium, with a large number of test particle return cycles, a power-law particle momentum distribution forms. For the number of particles with momentum greater than p (i.e., the integral spectrum, $F(p)$) at the shock wave front we have

$$F(p) \propto p^{-\Gamma} , \qquad \Gamma = \frac{3u_2}{u_1 - u_2}$$

in the interval from the injection momentum to the maximum momentum determined by the number of cycles passed by the given point in time [158]. The heart of the mechanism is in the regular energy gain at each intersection of the jump in the scatterers' velocity at the shock wave front and in the formation of a power-law spectrum due to the probability distribution of the number of particle returns [155, 159, 160]. Such a mechanism has a high efficiency of plasma flow energy transfer to the accelerated particles at the strong shock wave front. During acceleration, this mechanism forms power-law spectra of energetic particles, the exponents of which in the test particle model depend only on the ratio of the velocities of the scattering centers in the rest frame of the shock wave front. If the scattering centers do not have their own velocity relative to the plasma flow, then this ratio is the degree of plasma compression in the shock wave. For a strong shock wave in a nonrelativistic plasma, in this case, $u_1/u_2 = 4$, and $\Gamma = 1$. Differential spectrum of particles $\Phi(p) = \mathrm{d}F/\mathrm{d}p \propto p^{-\Gamma-1}$. In simulations of CR radiation and other problems, use is often made of the particle distribution function in phase space; in what follows, we denote it by $f(p)$ and have the relation $\mathrm{d}N = f(p)\, 4\pi p^2\, \mathrm{d}p = \Phi(p)\, \mathrm{d}p$.

The simplified probabilistic analysis of test particle scattering considered above implies a preliminary solution to the injection problem, i.e., the problem of separating the fraction of background particles that have entered the shock wave acceleration regime. Fermi [18, 145] pointed out the seriousness of the injection problem due to strong ionization energy losses by suprathermal particles. The modern PIC models considered above have demonstrated the possibility of injecting particles into acceleration mechanisms as an integral part of nonlinear processes of production of the viscous jump and the structure of collisionless shock waves (see Figs 4 and 5). Under conditions of a low Coulomb collision frequency, strongly fluctuating electric and magnetic fields caused by instabilities of the supersonic and super-Alfven plasma flow in the SW, along with plasma heating, produce a nonthermal particle distribution. A consistent solution to the problems of injection and formation of magnetic inhomogeneities that scatter energetic particles in space particle accelerators requires kinetic modeling of the interaction of the background plasma and the population of nonthermal particles on a scale with a dynamic range inaccessible to present-day computers. Monte Carlo simulation [23, 164–167] is a natural development of the probabilistic description discussed above and allows one to construct stationary nonlinear models of CR-modified SWs in accelerators with high particle acceleration efficiency.

5.2 Monte Carlo simulation of shock waves modified by accelerated particles

The nature of particle scatterers in a simple probabilistic model is not specified, which is sufficient to determine the asymptotic form of the spectrum in the one-dimensional problem. The efficiency of the acceleration mechanism is manifested, in particular, in the fact that the index of the differential spectrum of accelerated test particles (i.e., calculated without including the feedback effect of CRs on a flow with an SW) $(-\Gamma - 1)$, as shown above, for a strong shock wave tends to 2. This leads to a logarithmic increase in the pressure of relativistic particles $P_{\mathrm{CR}} \propto \ln(p_{\max}/p_0)$ with increasing highest accelerated particle momentum $p_{\max}$. Since suprathermal energetic CR particles can escape upstream, the CR pressure gradient can slow down the incoming plasma flow and modify the structure of the shock wave flow. Figure 6 schematically shows the effect of plasma flow modification by the pressure of accelerated particles that penetrate the plasma flow inflowing onto the shock wave front. The red dashed lines show the flow velocity profile in the rest frame of the front of the SW not disturbed by cosmic rays. It has the form of a velocity jump with $u_1/u_2 = 4$. The blue solid lines show the profile of the SW disturbed by CRs. The velocity of the plasma flow impinging on the front, carrying magnetic inhomogeneities, is slowed down by the ponderomotive force caused by the CR pressure gradient. The CR density distribution is shown here by the green solid line. The magnitude of the viscous velocity jump in the shock wave modified by the CRs is appreciably smaller than in the undisturbed SW. Figure 6a serves to illustrate the model of modification of the CR particle momentum distribution function at the SW front. The red line schematically shows the particle distribution function in the phase space $f(p)$ (i.e.,

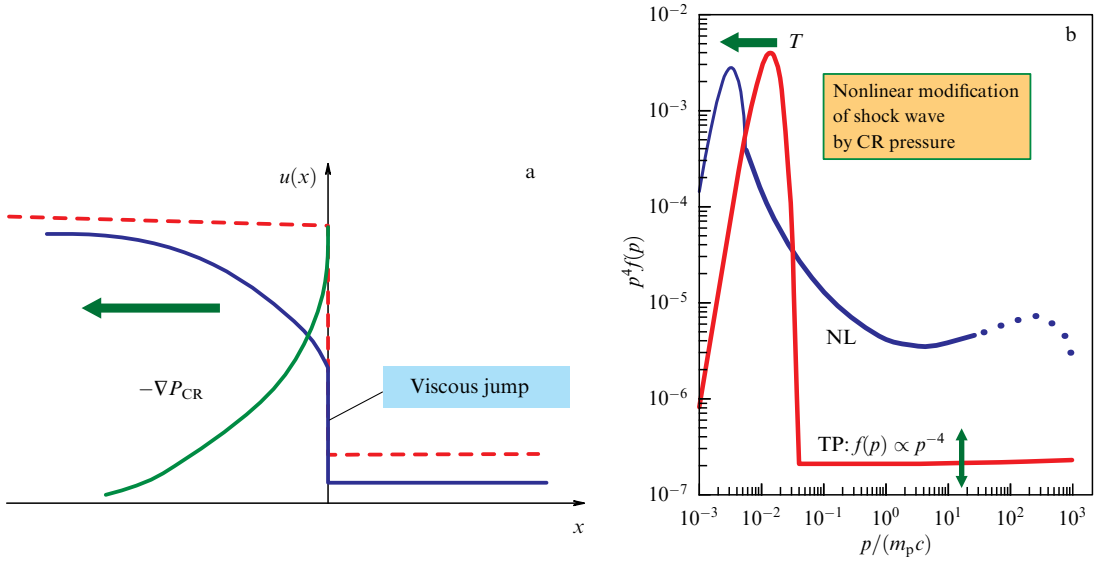

Figure 6. (a) Schematic illustrating structure of strong collisionless SW modified by pressure of accelerated particles. Red dashed line shows what shock wave flow profile would look like without including its modification by CR pressure gradient. Blue line shows shock wave profile with inclusion of slowing-down of incoming plasma flow by cosmic rays accelerated by it. Pressure profile of accelerated particles themselves is shown by green curve. (b) Shapes of accelerated particle spectra. Spectra calculated in test particle model are shown by red lines, and those calculated with inclusion of nonlinear flow modification are shown by blue curves.

the CR spectrum), related to the previously introduced spectral function as $\mathrm{d}F/\mathrm{d}p = 4\pi p^2 f(p)$. The distribution has two components: a thermal peak and a nonthermal power spectrum. The slowing-down of the shock upstream flow by CR pressure (see the velocity profile shown by the blue line in Fig. 6a) in the case of a sufficient injection rate and effective Fermi acceleration modifies the particle distribution function. The temperature of the quasi-Maxwellian component decreases due to the transfer of part of the plasma flow energy flux into the CRs and due to the increase in the total plasma compression ratio (asymptotic ratio $u_1/u_2 > 4$). The coordinate dependence of the velocity profile of scattering centers in the shock upstream flow leads to a deviation from the power law of the high-energy CR distribution. The flow structure in collisionless SWs modified by accelerated CRs in Fig. 6 has a certain similarity with models of strong collisional radiative SWs discussed in the classical monograph by Ya.B. Zel'dovich and Yu.P. Raizer [161]. Radiation-modified SWs emerge on the surface of the supernova progenitor star and, as they propagate, transit to the collisionless shock wave regime of the supernova [162]. A significant distinction of modified SWs is the possibility of disappearance of the viscous jump in the radiative shock wave, while in the CR acceleration models the jump, although reduced compared to the unperturbed shock wave (see Fig. 6), remains finite, since CR injection occurs on it. In the models with CR reacceleration, continuous flows similar to radiative flows are probably possible. The main features of the qualitative analysis of Fig. 6 confirm the quantitative results obtained in the nonlinear Monte Carlo model [23, 163]. We will briefly discuss the processes of magnetic turbulence production as a key factor in the Fermi acceleration model.

The connection of cosmic rays with the background plasma flow is realized through the scattering of CRs by magnetic field inhomogeneities. While the proper velocities of scatterers relative to the plasma are of the order of the Alfven velocity in an unperturbed magnetic field, relative to the front of a strong shock wave with $M_a \gg 1$, they are transported with a velocity close to that of the background plasma.[3] Acceleration of particles by converging plasma flows in the diffusive mechanism of CR acceleration by shock waves is inevitably accompanied by the appearance of anisotropy in the momentum distribution of accelerated particles locally ahead of the shock front. Instabilities of anisotropic CR distributions are accompanied by amplification of background fluctuations of the magnetic field with scales both resonant (see [106, 168, 170]) and nonresonant [171] to the gyroradii of the accelerated particles.

Nonlinear Monte Carlo simulation of CR acceleration by a strong shock wave [23, 163] implements an iterative scheme, at each step of which the entire particle distribution function is calculated as a function of the particle coordinate and momentum, without separating the particles into thermal and nonthermal components. The particle distribution is nonequilibrium and anisotropic. The growth rate of magnetic fluctuations is calculated based on quasi-linear dispersion relations [169–171]. It is significant that the change in the magnetic field among two successive iterations should be small, which justifies the possibility of using quasi-linear relations. The fluctuation spectrum determines the energy balance equation among the growth of fluctuations, nonlinear energy transfer along the spectrum, and mode dissipation. Based on the simulation of turbulence, determined are the momentum dependent mean free paths of particles, which is a key element of particle transport in the Monte Carlo model. Macroscopic plasma velocities are defined as moments of the particle distribution function, with the velocities of scatterers (magnetic fluctuations) relative to the plasma being calculated. Iterations are performed until a distribution function is found that satisfies the conservation laws of total energy and momentum flows in a stationary SW. The presence of stationary solutions is provided by a balance

[3] Electric currents of accelerated particles escaping from the acceleration region can significantly enhance the magnetic fields. Then, the velocity of scatterers can differ significantly from the velocity of the background plasma.

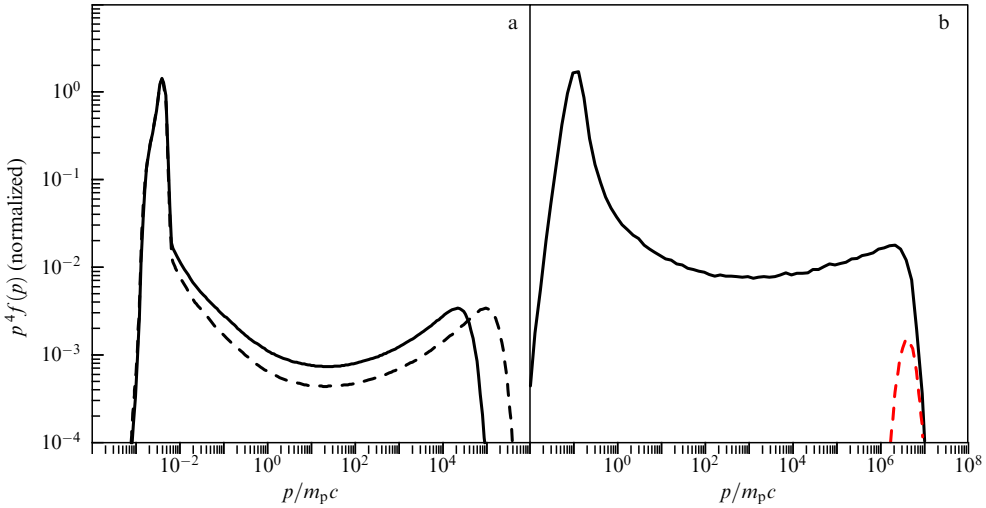

Figure 7. Stationary spectra of protons accelerated by strong plane SWs calculated using Monte Carlo method. Model includes nonlinear effects of plasma flow deceleration, flowing onto shock front, and amplification of fluctuating magnetic fields by anisotropic accelerated particle distributions in shock pre-front [23]. (a) Results of model simulations of CR spectra of young supernova remnants Cassiopeia A (solid curve) and Tycho Brahe (dashed curve). These two supernova remnants have similar shock velocities of the order of 4000 km s^{-1}, but different radii. (b) Spectrum of protons accelerated by SW traveling with velocity of $\sim 0.2\,c$. Shock waves of this type are considered in Section 7.1 to be a source of CRs and nonthermal radiation in extended X-ray jet of microquasar SS433. Red dashed curve shows spectrum of protons escaping from accelerator towards plasma flowing onto SW.

between the influx of kinetic energy of particles with the unperturbed plasma flow and the escape from the system of accelerated CRs that have reached the free escape boundary determined by the physical size of the accelerator.

The mechanisms of magnetic turbulence production in the SW prefront allow one to describe the particle scattering processes; these mechanisms are included in Monte Carlo models along with the nonlinear modification of the one-dimensional flow by the CR pressure gradient [23, 163]. As shown in Fig. 6b, the momentum distribution of particles accelerated by a plane SW (with a flow modified by accelerated nonthermal particles) has a concave spectrum that differs from the power-law distribution of the test particle model described above (the red solid line in Fig. 6b). Figure 7 shows the model spectra of particles accelerated by a plane modified SW, which were simulated using the nonlinear Monte Carlo model for parameters corresponding to the SWs of young SNe remnants Cassiopeia A and Tycho Brahe (Fig. 7a). Figure 7b shows the particle distribution formed by a shock wave with a subrelativistic velocity of $\sim 0.2\,c$, which is characteristic of extended jets of the microquasar SS 433 (see Section 7.1 below). Model spectra of electrons and nuclei allow us to calculate the expected spectra and images of SN remnants in the radio, X-ray, and gamma-ray ranges, as well as high-energy neutrino fluxes. A comparison with observations makes it possible to test the adequacy of very complex models of cosmic particle accelerators.

6. X-ray radiation from supernova remnants

Based on the first X-ray observations, Ginzburg and Syrovatskii [172] noted the possibility of a synchrotron (magnetic bremsstrahlung) origin for the X-ray radiation from the Crab Nebula. Today, it has been determined that the synchrotron radiation from the Crab Nebula produced by the powerful relativistic wind of the PSR B0531 + 21 pulsar, a remnant of the SN 1054 supernova, extends to energies of about 100 MeV (and even higher during outbursts) [16]. Based on a model extrapolation of radio observations of the synchrotron radiation from the shell of the supernova SN 1006, the authors of Ref. [173] demonstrated the possibility of detecting the synchrotron radiation from this supernova in the X-ray range. Observations by the Chandra X-ray Observatory have allowed the construction of images of extended young supernova remnants with an angular resolution of about an arcsecond. The combination of the unprecedented angular resolution and high sensitivity of the Chandra observatory has made it possible to detect thin bright X-ray filaments at the outer edges of the X-ray shell in images in the photon energy range of 4–6 keV. In this energy range, the contribution of K-shell lines of abundant chemical elements is small, and continuous emission prevails in the bright filaments. The power-law spectrum of this emission indicated its synchrotron nature, in accordance with the predictions of Ref. [173]. In some cases, the observed X-ray profiles have a width of several arc seconds, which is significantly narrower than the observed synchrotron radio profiles of the envelopes of young supernova remnants, such as Cassiopeia A, Tycho Brahe, SN 1006, and RXJ J1713.7-3946. The narrowness of the synchrotron X-ray filaments cannot be explained by a rapid drop in the magnetic field behind the front of the outer shock wave of the supernova, since then, the width of the radio envelope would be the same. The difference in widths is probably due to the narrow distribution of ultrarelativistic electrons with energies above TeV accelerated by the fast shock wave. The rate of electron energy loss to synchrotron and Compton radiation $\propto p^2$ [14], which determines the difference in the width of the radiation region Δ behind the shock front as function of the synchrotron photon energy $E_{\rm ph}$.

The value of Δ depends on the nature of particle transport in the flow behind the SW front. This value is found by solving the transport equation, which includes the diffusion and advection of relativistic electrons. The CR diffusion coefficient is determined by the evolution of strong turbulence behind the strong SW front, the source of which is the instabilities caused by the anisotropy of accelerated relativis-

tic protons. In the theory of CR diffusion acceleration by shock waves, a simplified parametric specification of the particle diffusion coefficient $D(p)$ in strong turbulence is often used with $D(p) = \eta c^2 p/(ZeB)$, where B is the amplitude of the turbulent magnetic field (the so-called Bohm diffusion). If the diffusion coefficient is small, i.e., $D(p) < u_2 \Delta$, then the transport of electrons emitting synchrotron X-ray radiation is caused by advection. In this case, measuring the width of the X-ray filament Δ in the energy range around $E_{\rm ph}$ allows us to estimate the magnetic field strength using the relation [56]

$$B_2 \approx 178 \left[\frac{\Delta}{10^{17}\ \mathrm{cm}}\right]^{-2/3} \left[\frac{E_{\rm ph}}{1\ \mathrm{keV}}\right]^{-1/3} \times \left[\frac{u_1}{4u_2}\right]^{-2/3} \left[\frac{u_2}{5000\ \mathrm{km\,s^{-1}}}\right]^{2/3} \mu\mathrm{G}\,. \quad (6)$$

Estimates of the magnetic field behind the front of a strong SW are usually made on the basis of a relation that assumes that the highest energies of SW-accelerated electrons are determined by their energy losses, and not by the size of the pre-front, as is the case of protons. In this case, the diffusion and advection lengths are close, and an estimate of the field can be obtained from

$$B_2 \approx 110\,\eta^{1/3} \left[\frac{\Delta}{10^{17}\ \mathrm{cm}}\right]^{-2/3} \mu\mathrm{G}\,. \quad (7)$$

The values of the magnetic field based on the widths of synchrotron X-ray filaments measured by the Chandra Observatory are given in Ref. [174]. The filament sizes are $\Delta \sim 5 \times 10^{16}$ cm, and magnetic fields with a strength above 200 μG behind the shock front of the Cassiopeia A and Tycho Brahe SN remnants are calculated from observational data. As examples of young SN remnants, we consider two remnants. The first is Cassiopeia A, an SN IIb remnant with an estimated age of ~ 340 years and a radius of ~ 1.7 pc located at a distance of ~ 3.4 kpc [175]. The second object is a type Ia SN remnant discovered by Tycho Brahe in 1572. The distance to Tycho Brahe's SN is estimated (with large uncertainties) at ~ 3 kpc; the angular diameter of this remnant is $\sim 8'$. The velocities of the expanding shells in both remnants are ~ 5000 km s^{-1}.

The resultant magnetic field strengths in both young remnants of different types are an order of magnitude higher than the values expected from adiabatic compression of the components of the interstellar magnetic field transverse to the normal to the SW. High turbulent magnetic field strengths can be obtained due to the mechanisms of amplification of background field fluctuations by instabilities associated with the anisotropy and nonuniformity of the distribution of accelerated CRs in the SW pre-front [169–171]. The magnetic fluctuations amplified in the pre-front then undergo additional compression at the SW front.

The energies of the accelerated electrons that form the synchrotron filaments of Cassiopeia A and Tycho Brahe are of the order of 20 TeV. Therefore, the high-angular-resolution X-ray observations from the Chandra observatory made it possible to estimate the energies of the accelerated particles within the synchrotron model, and the maximum energies of the accelerated protons can be higher than 20 TeV, since the synchrotron energy losses of the protons are small. The resultant values correspond to the highest energies of the particles accelerated by the SN SWs, calculated with the nonlinear Monte Carlo model for SW velocities higher than 3000 km s^{-1} (see Fig. 7a and Ref. [23]).

6.1 Polarized X-ray radiation from young supernova remnants

The observed synchrotron X-ray fluxes from young supernova remnants are high enough [176] to measure the polarization of X-ray emission by gas-pixel detectors of the orbital observatory IXPE (Imaging X-ray Polarimetry Explorer) launched in December 2021. Polarized X-ray emission has been successfully measured from supernova remnants Cassiopeia A [177], Tycho Brahe [178], SN 1006 [179], RX J1713.7-3946 [180], etc.

Figure 8 from Ref. [178] shows a significance map of polarized X-ray emission detection from the Tycho Brahe SN remnant (Fig. 8a), and the map in Fig. 8b presents the polarization vectors and polarization degree obtained from the analysis of observations. The IXPE maps are superimposed on the X-ray radiation contours in the 4–6 keV range measured by the Chandra Observatory. IXPE observations have revealed the presence of regions with a high degree of polarization, for example $23\% \pm 4\%$, in the western part of the Tycho Brahe SN remnant. Of particular interest are the directions of the polarization vectors shown in Fig. 8b. According to the theory of synchrotron radiation [14, 15], the measured polarization directions correspond predominantly to the radial directions of the magnetic field in the region of radiation production behind the shock front. Strong SN shocks compress the plasma of the interstellar medium and adiabatically enhance the magnetic field components transverse to the normal to the shock. Observations of Tycho Brahe's SN described above, Cassiopeia A [177], SN 1006 [179], and some regions in RX J1713.7-3946 [180] yielded the opposite result: a magnetic field directed locally along the normal of the shock wave, i.e., radial for a spherical SN remnant. On the other hand, we noted earlier that the observed high magnetic field strengths behind the SW fronts of these SNs cannot be obtained by adiabatic compression of the plasma in the SW either. Hard spectra of protons accelerated by the diffusive mechanism on an SW of SNe provide a large value of the free energy of the anisotropic CR distribution subject to instabilities. Fluctuating magnetic fields can be enhanced by mechanisms associated with instabilities of the anisotropic CR distributions accelerated by strong shock waves of SN remnants. The nonlinear models of diffusive acceleration of particles by the SW considered above allow the conversion of $\gtrsim 10\%$ of the kinetic energy flux of the plasma flowing onto the SW front (in the rest frame of the SW) into CRs. The subsequent transition of several percent of the CR energy density into magnetic fields enhanced by CR instabilities allows the observed values of field strength to be achieved.

The observed high degree of polarization of X-ray radiation from an SN remnant with a highly turbulent field is explained in the model of CR acceleration by shock waves by the significant anisotropy of magnetic turbulence enhanced by instability of anisotropic CR distributions. The nonresonant Bell instability caused by the current of CRs escaping the SW of the SN remnant enhances, in the pre-front of the SW, magnetic fluctuations with wavelengths shorter than the gyroradius of the escaping CRs [169–171, 181]. The interaction of magnetic fluctuations enhanced by the Bell instability with the SW front is shown in Fig. 9a, which presents the results of MHD modeling of this process [182].

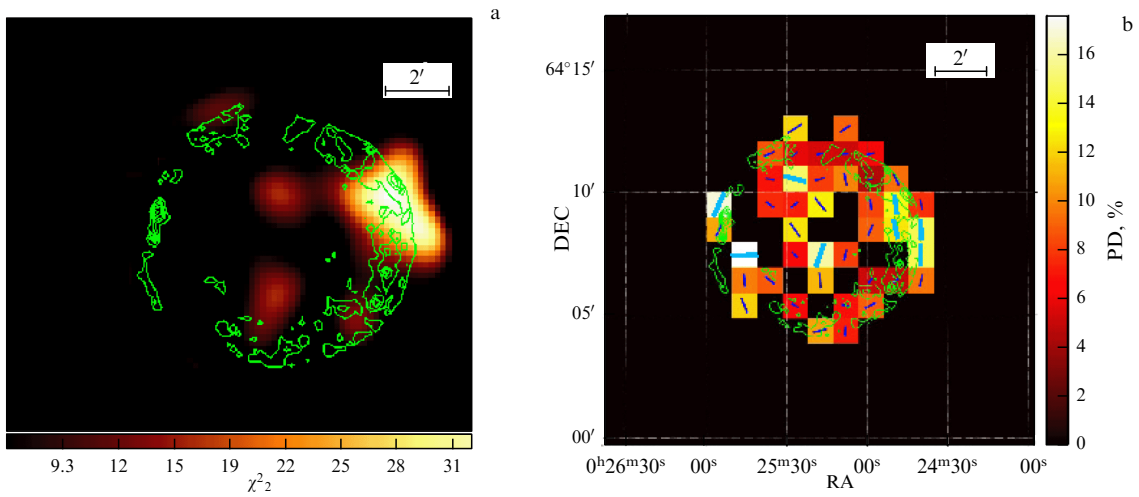

Figure 8. (a) Detection significance map of polarized X-ray emission from Tycho Brahe SN remnant, smoothed with 10.4″ kernel Gaussian filter, obtained by IXPE [178]. (b) Map of polarized X-ray emission in 3–6 keV range, with 60″ pixel size, obtained by IXPE. Color bar on right shows degree of polarization. Blue lines show direction of polarization vector (electric field of radiation). Local direction of magnetic field in SN remnant is orthogonal to polarization vector. Green contours show emission map in 4–6-keV range constructed by Chandra Observatory. (IXPE images borrowed from Ref. [178] with kind permission of Dr.R. Ferrazzoli.)

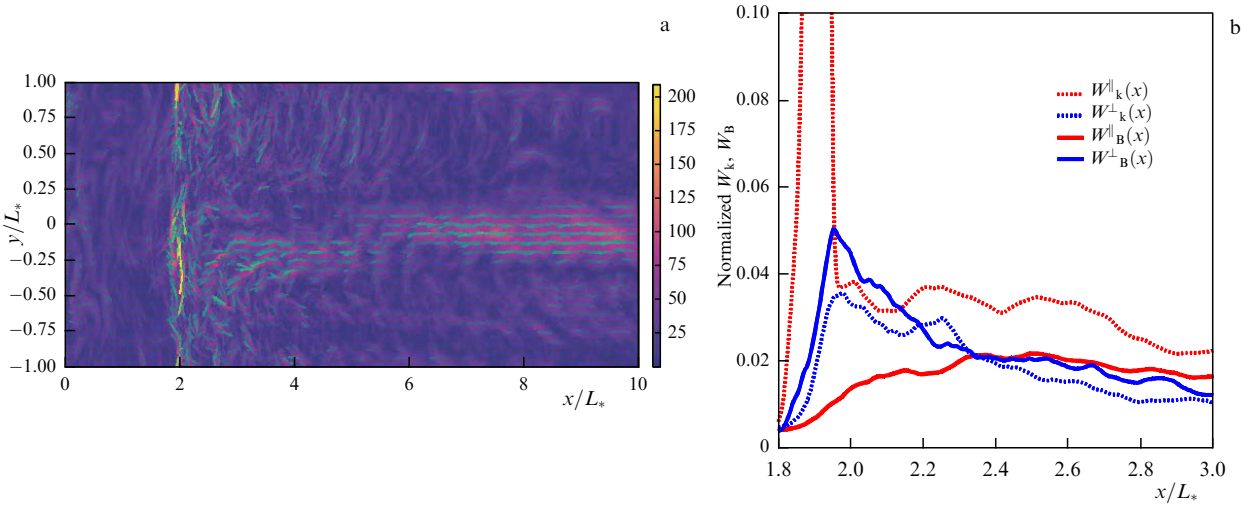

Figure 9. (a) Spatial distribution of magnetic field during passage of magnetic turbulence through SW front; turbulence is initiated by nonresonant Bell instability in plasma flow impinging on shock front. Region of SW front curved by interaction with density fluctuations is clearly visible. Compression of transverse components of magnetic field behind SW front is replaced downstream by an increase in longitudinal components of magnetic field with respect to flow [182]. (b) Energy density of turbulence behind SW front normalized to value of kinetic energy density of unperturbed flow impinging on SW front. Dotted curves show kinetic energy densities of plasma motions, and solid curves show energy density of magnetic field. Radial component of magnetic field is solid red curve, and transverse component of field is solid blue curve. In decaying turbulence behind SW front, visible are a relative increase in radial magnetic component and its predominance over transverse component with increasing distance from SW. Strong disturbances of SW front lead to radial anisotropy of magnetic turbulence behind SW front [182].

Figure 9b serves to illustrate the production mechanism of magnetic fields, predominantly directed along the plasma flow velocity behind the SW. The nonlinear evolution of enhanced magnetic field fluctuations is accompanied by the formation of strong density fluctuations in the region ahead of the SW front. The interaction of such density fluctuations with a thin viscous SW jump generates intense anisotropic turbulence of plasma velocity vortices behind the SW front. As the free anisotropic vortex turbulence decays receding from the SW front, it amplifies magnetic fluctuations by the Kazantsev dynamo mechanism. In this case, a predominantly radially oriented turbulent magnetic field is produced in the fast SWs of young SN remnants [182]. Figure 10 from Ref. [182] shows the degree of X-ray polarization of synchrotron radiation as a function of the radius inside a spherical SN remnant simulated within the framework of the approach described above. The model allows obtaining polarization degrees higher than 20% for SN remnants with parameters corresponding to young SN remnants. An important feature of the model is the sensitive dependence of the degree and direction of polarization of X-ray radiation on the scale of turbulence generated by the Bell instability of CRs. The scale of magnetic turbulence is orders of magnitude lower than the spatial resolution of the IXPE detector. However, measuring the polarization allows testing turbulent plasma processes even on small spatial scales that are not resolved by IXPE. High-angular-resolution X-ray observations with the Chandra Observatory together with measurements of the polarization of X-ray emission from young SN remnants by IXPE detectors have provided unique information on particle acceleration in SN remnants.

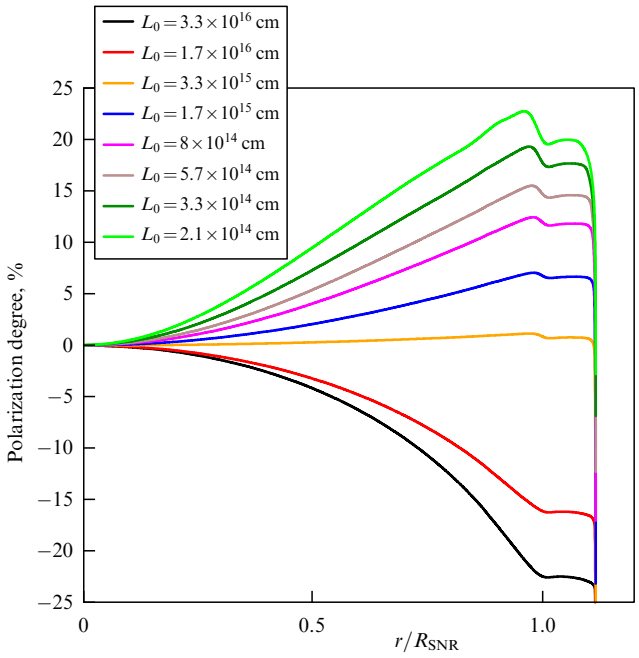

Figure 10. Polarization degree of X-ray radiation of SN remnant as a function of radius, normalized to radius of SW [182]. Polarization profiles were calculated for different values of the main scale L_0 of Bell turbulence. Fraction of synchrotron photons relative to thermal photons was assumed to be 0.6. Positive and negative values of polarization degree correspond to transverse and radial directions of radiation polarization (electric field of photons), respectively.

7. Gamma-ray emission from supernova remnants

Observing gamma-ray emission from high-energy CRs is a natural way to test both hypotheses about the nature of CR sources and models of CR propagation in the Galaxy [14, 24, 25, 29, 183]. The H.E.S.S., MAGIC, VERITAS, HAWC, LHAASO, Taiga, and Fermi modern gamma-ray observatories have achieved sensitivity that allows the detection of gamma-ray emission from SN remnants in the Galaxy and Magellanic Clouds. Reviews of some results of observations of gamma-ray emission from supernova remnants can be found in Refs [56, 96, 174, 184, 185].

More than 70 years ago, synchrotron radio emission from SN remnants was discovered, proving the acceleration of relativistic electrons with energies in the GeV range, which formed the basis of Ginzburg and Syrovatskii's theory of the origin of cosmic rays [14]. One of the tasks of gamma-ray astronomy is searching for direct evidence of proton acceleration in SN remnants. Although gamma rays from supernova remnants were detected in the mid-1960s, it was not possible to reliably separate the radiation of electrons and positrons from the radiation of protons. Inelastic collisions of relativistic CR protons with interstellar gas are accompanied by the production of π^0-mesons, whose decay in the pion rest frame produces two photons with energies of about 67.5 MeV. The radiation of relativistic protons with a power-law spectrum in inelastic p–p collisions has a characteristic peak in the spectral distribution of the photon energy, lying in the energy range between 100 MeV and several GeV. The shape of the peak depends on the spectral index of the relativistic proton distribution (see, for example, Ref. [186]). The middle-aged SN remnants IC 443 and W44 (their age is more than 10,000 years) have a high luminosity in the GeV range with an energy flux of $\sim 10^{-10}$ erg cm^{-2} s^{-1}, which is due to their interaction with a dense environment in the form of molecular clouds. Observations of IC 443 and W44 with the AGILE gamma-rays telescope and the Fermi observatory made it possible to detect for the first time a feature in the radiation spectrum above 100 MeV [187, 188]. The observed spectrum of gamma rays is compatible with that expected from radiation in pp-interactions of accelerated protons. To reliably separate the contribution of proton radiation from the bremsstrahlung of primary and secondary electrons, spectrum measurements at energies below 100 MeV are needed, but today this is a complex problem for detector technologies.

Observations of gamma rays from young supernova remnants are used to estimate the nature of particle acceleration mechanisms and their contribution to the observed spectrum of galactic CRs. An important role here is played by determining the spectra and highest energies of particles accelerated in the SN remnant. Gamma-ray radiation from IC 443 and W44 above 10 GeV has a soft spectrum photon index > 2, which distinguishes these sources from the younger SN remnants of Cassiopeia A, Tycho Brahe, RX J713.7-3946, and RX J0852.0-4622. In particular, the highly interesting SN remnant RX J1713.7-3946 (see, for example, Ref. [189]) has a hard photon index of ~ 1.5 in the GeV range, and ~ 2 for energies above TeV. One-zone models of RX J1713.7-3946 allow explaining the observed hard index by Compton radiation of electrons accelerated by a strong shock of the SN [190]. However, there are observational indications of a more complex, multi-band structure of RX J1713.7-3946 [180, 191], including the possible interaction of individual parts of the SN remnant with a dense molecular gas. According to an estimate based on the model of Ref. [192], which includes radiation from both nuclear interactions and Compton scatterings of accelerated leptons, the ratio of contributions to the observed flux from proton and electron radiation may be 6:4.

The RX J1713.7-3946 SN remnant, which is located in the southern sky, has a weak radio flux, and high-sensitivity X-ray observations have revealed a complex configuration of shock waves in different regions of RX J1713.7-3946 with a wide range of velocities from 900 to 4000 km s^{-1} [191]. The youngest galactic SN remnant, G1.9 + 0.3, with an estimated age of about 100 years, has an SW velocity of $\sim$ 14,000 km s^{-1} [193]. Interestingly, a comparison of the nonthermal X-ray spectra of RX J1713.7-3946 and G1.9 + 0.3 performed in Ref. [194] suggested that the rate of electron acceleration in G1.9 + 0.3 is probably significantly lower than in RX J1713.7-3946, despite the higher estimated shock velocity. This suggests that the shock velocity is not the only factor determining the acceleration rate and highest accelerated particle energies. Gamma-ray radiation from G1.9 + 0.3 has not yet been measured.

Due to the limited spatial resolution of the detectors, the use of observed gamma-ray spectra for detailed testing of the predictions of the particle acceleration models discussed above is a highly intricate task. The detected gamma-ray fluxes from SN remnants generally include contributions from radiation of both relativistic nuclei and electrons captured in the accelerator, and CRs that left the SN at different stages of the remnant's evolution. An example is provided by the spectrum of high-sensitivity long-term observations of the Cassiopeia A SN remnant by the Fermi and LHAASO observatories [195], which is shown in Fig. 11. The shape of the spectrum can be explained by the radiation of protons accelerated by the SW of the remnant, with a

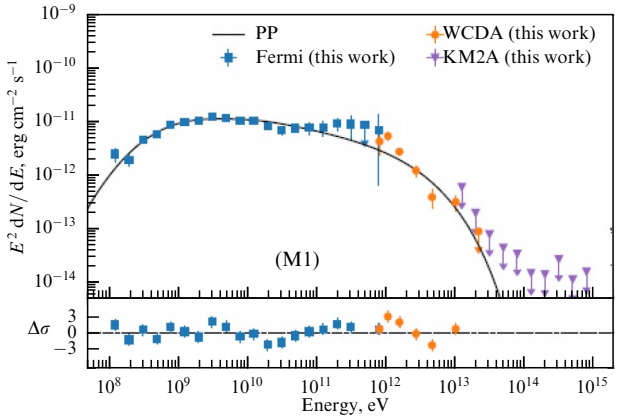

Figure 11. Gamma-ray spectrum of Cassiopeia A young SN remnant based on long-term observations with Fermi observatory and ground-based LHAASO [195].

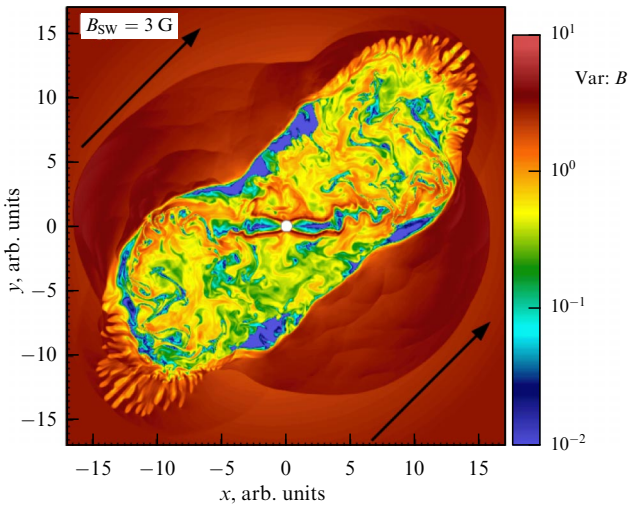

Figure 12. Model of the interaction region of a relativistic pulsar wind and a strongly magnetized wind of a young massive star in a binary system. The local map of magnetic fields is shown, the magnitudes of which are given on the color bar on the right. The magnetic field of the wind of a massive star is taken to be 3 Gauss, which is possible at an orbital phase with a distance between the stars up to ten of AU.

possible indication of a concave-convex spectrum of high-energy particles. Such a spectrum corresponds to the predictions of the SW proton acceleration models presented in Fig. 6 and Fig. 7a. The concave-convex shape of the proton spectrum is due to the nonlinear modification of the SW. On the other hand, it is also possible to explain the observations by a combination of contributions from the nuclear and electron components [195]. The gamma-ray spectra of another young SN remnant, Tycho Brahe [196], whose model proton spectra are shown in Fig. 7a, can be explained by a combined contribution by radiation of nuclei and Compton radiation by electrons [197].

Taken together, observations of nonthermal radiation from RX J1713.7-3946 and some other young SN remnants give ground to estimate the maximum energies of particles accelerated in them as values of the order of 100 TeV, and the total energy of nuclei accelerated in them as $\sim 10^{50}$ erg [184, 198], which fully corresponds to the provisions of the theory of the CR origin [14]. Observations of young SN remnants do not provide an answer to the question of the origin of CR in the energy range about PeV and beyond the knee in the spectrum. Scenarios of particle acceleration in the early stages of the evolution of supernovae with an age of up to several years are possible, for example, in the presence of a dense circumstellar envelope created by the wind of red supergiant stars [80, 82, 199, 200], or by moderately relativistic shocks waves of rare classes of relativistic supernovae [96, 97, 117]. Observations of gamma-ray emission from very young SNs in nearby galaxies, such as SN 2023ikf [86] discussed above, are still very rare.

On the other hand, the high sensitivity and accumulated long-time exposures of the gamma-ray observatories H.E.S.S., HAWC, and LHAASO made it possible to detect radiation fluxes of $\sim 10^{-13}$ erg cm^{-2} s^{-1} and lower, with LHAASO detecting photons with energies above 100 TeV, and this opened up the possibility of searching for PeV-regime CR accelerators among binary stars with relativistic SN remnants.

7.1 Particle acceleration in binary gamma-ray sources

Gamma-ray radiation with energies above 100 TeV range is observed from binary star systems, one of whose companions is a compact SN remnant, a young pulsar (for example, LS I + 61° 303), or an accreting stellar-mass black hole (SS 433), and the second is a massive star of an early spectral class O or B. Such objects (in the case of a black hole companion, they are called microquasars) are produced as a result of SN outbursts in binary systems with massive stars.

The nature of the relativistic companion in LS5039, unlike the similar source LS I + 61° 303, has not yet been clearly determined, although many characteristics are compatible with the presence of a young pulsar in the system. The gamma-ray spectrum of LS5039, detected by the HAWC observatory [201], has a relatively soft photon index of 2.7–2.8, but shows no signs of a spectrum roll-off up to the highest measured energy of 100 TeV. This indicates acceleration of protons in the radiation source to energies slightly above a PeV. In the binary system LS I + 61° 303, preliminary LHAASO data showed spectra similar to those of LS5039 in the energy region above 10 TeV.

Theoretical models demonstrate the possibility of accelerating protons to energies of the order of a PeV in binary systems where the relativistic wind of a pulsar collides with the wind of an early spectral type star. Figure 12 shows the results of relativistic MHD simulations of the structure of the domain of the winds collision [202]. The results of direct integration of the equation of motion of protons injected with an energy of ~ 200 TeV into the system of colliding winds showed the possibility of confining such particles in the system and accelerating them to energies above a PeV, which is illustrated in Fig. 13a. Figure 13b shows the time evolution of the proton spectrum in the PeV range in a binary system with a pulsar. The condition for the possibility of accelerating protons to PeV energies is the presence of a magnetic field of the order of 1 G in the plasma of the wind of a massive star [202]. In this case, the spectrum of proton energies sets in over a time of the order of several hours.

Recent observations of high-energy gamma-ray emission from the galactic microquasar SS433 [203–206] have detected a source of photons with energies significantly higher than 100 TeV, which coincides well with a jet extending tens of parsecs from the black hole, previously discovered as a source of nonthermal synchrotron X-ray radiation (see, for example, Refs [207, 208]). Microquasar SS 433 was discovered more than 40 years ago, and observations of its multichannels over

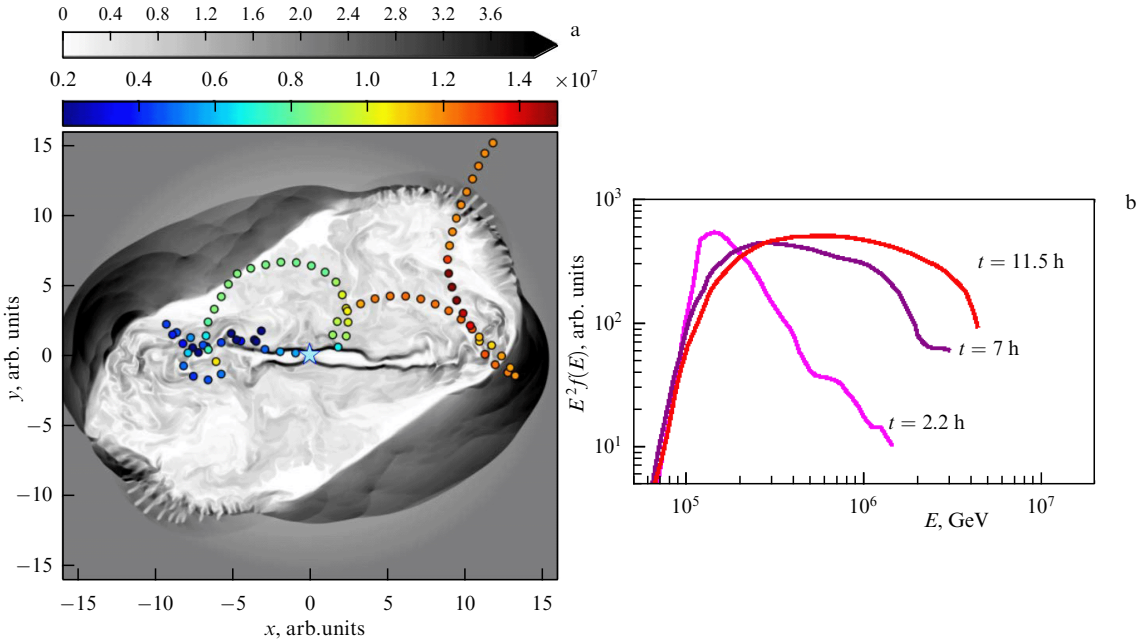

Figure 13. Illustration of proton acceleration to energies of the order of a PeV in a binary system with interaction of relativistic wind of pulsar and wind of young massive star of class O or B with strong magnetic field (see Fig. 12). (a) Gain in particle energy in particle trajectory obtained by integrating equation of motion in region of wind collision. Color scale shows proton Lorentz factor measured in units of 10^7. Calculation shows possibility of confining and accelerating particles with energies of the order of a PeV in the system. (b) Time evolution of spectrum of initially monoenergetic particles injected into the system. Time in figure is expressed in hours. (Model is described in detail in Ref. [202].)

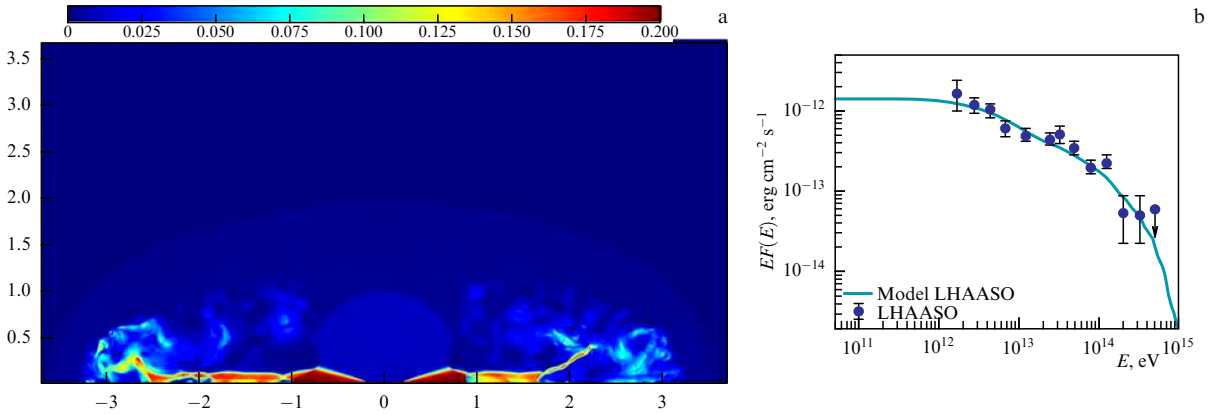

Figure 14. (a) Velocity field map in magnetohydrodynamic model of extended X-ray jet structure in microquasar SS 433. Source of outflows is accretion disk of black hole at center of system. Color scale shows plasma velocities in units of speed of light. Jet recollimation shocks accelerate particles to energies of the order of a PeV (Fig. 7b). (b) Compton gamma-ray spectrum of electrons accelerated by SWs along with results of gamma-ray flux measurements of SS433/W50 using LHAASO observatory borrowed from Ref. [203].

these years have provided unique information about the nature and properties of the object (see, in particular, the detailed review Ref. [119]). The observational data are consistent with models of supercritical accretion onto a black hole with a mass of several solar masses, which fosters a plasma outflow power from the accretion disk of the order of 10^{40} erg s^{-1}. The observed morphology of the extended X-ray jet lends itself to explanation by model [118], in which the outflow from the precessing accretion disk has two components: a polar wind that is quasi-spherical or has a wide cone of angles, and a narrowly collimated wind with an opening angle of about 10°, a plasma flow velocity of ~ 0.2–$0.3\,c$, and a kinetic power that constitutes a significant fraction of the total power of the system. Simulations [118] suggest that the intersection of the polar wind termination surface by the collimated flow is accompanied by the production of strong SWs in the collimated flow. The models of particle acceleration and magnetic field amplification by shock waves within the framework of the Fermi diffusion mechanism, which were considered in Section 5.2, are applicable to SWs in a collimated flow with a plasma velocity of about $0.2\,c$ in the W50/SS433 source (Fig. 14a).

Figure 14a shows the results of simulations of the collision of the plasma outflows which were described above in two directions from the black hole located at the center. Magnetohydrodynamic simulations revealed regions of production of strong SWs in the plasma flow at a distance of more than 10 pc from the black hole. Figure 7b shows the spectrum of protons accelerated by shocks in an extended collimated wind, which was calculated using the nonlinear kinetic Monte Carlo model described in detail in Ref. [23]. The spectrum of Compton gamma-ray radiation of ultra-

relativistic electrons accelerated, like protons, to energies of the order of a PeV[4] is shown in Fig. 14b in comparison with the LHAASO observational data presented in Ref. [203]. Synchrotron radiation of electrons accelerated by an SW in a narrow collimated wind allows a description of the results of X-ray observations of an extended source obtained by the orbital X-ray observatories Chandra, XMM-Newton, NuSTAR, and IXPE, presented in Refs [207, 208]. The acceleration of protons to energies of several PeV with a power conversion efficiency of the order of 10% into accelerated high-energy CRs will allow the component of galactic CRs after the spectrum kink to be explained by the contribution of several binary gamma-ray sources of this type.

The potential of operating gamma-ray observatories, the results of which we briefly discussed above, together with detectors being constructed, such as the Taiga-100 observatory [209], gives hope for significant progress in the search for CR sources with energies above one PeV. This will be another element of the picture of the origin of cosmic rays, the essential elements of which were developed by V.L. Ginzburg, S.I. Syrovatskii, and their colleagues and students [14, 168].

This study was supported by the Russian Science Foundation under Grant No. 25-72-20007. The author expresses his appreciation to F.A. Aharonian, V.A. Dogiel, D.C. Ellison, J.A. Kropotina, L.A. Kuz'michev, K.P. Levenfish, S.M. Osipov, A.E. Petrov, V.I. Romansky, R. Treumann, S.V. Troitsky, and Yu.A. Uvarov for the informative discussions over the years and assistance in choosing illustrations, V.S. Mutina for assistance in finding a photograph, and Riccardo Ferrazzoli and P. Slane for the polarized image of Tycho Brahe's supernova remnant.

References

1. Hess V F *Phys. Z.* **13** 1084 (1912)
2. Skobelzyn D *Z. Phys.* **54** 686 (1929)
3. Skobeltzyn D V, in *Early History of Cosmic Ray Studies* (Astrophysics and Space Science Library, Vol. 118, Eds D V Skobeltzyn, Y Sekido, H Elliot) (Dordrecht: Springer, 1985) p. 47, https://doi.org/10.1007/978-94-009-5434-2_6
4. Anderson C D *Phys. Rev.* **43** 491 (1933)
5. Dorman I V *Kosmicheskie Luchi: Istoricheskii Ocherk* (Cosmic Rays: A Historical Essay) (Moscow: Nauka, 1981)
6. Toptygin I N *Phys. Usp.* **56** 417 (2013); *Usp. Fiz. Nauk* **183** 439 (2013)
7. Lidvansky A S *Phys. Usp.* **67** 943 (2024); *Usp. Fiz. Nauk* **194** 999 (2024)
8. Baade W, Zwicky F *Phys. Rev.* **46** 76 (1934)
9. Condon J J, Ransom S M *Essential Radio Astronomy* (Princeton, NJ: Princeton Univ. Press, 2016) https://doi.org/10.1515/9781400881161
10. Shklovskii I S *Dokl. Akad. Nauk SSSR* **90** 983 (1953)
11. Ginzburg V L *Dokl. Akad. Nauk SSSR* **92** 1133 (1953)
12. Ginzburg V L *Usp. Fiz. Nauk* **51** 343 (1953)
13. Ginzburg V L, Syrovatskii S I *Sov. Phys. Usp.* **3** 504 (1961); *Usp. Fiz. Nauk* **71** 411 (1960)
14. Ginzburg V L, Syrovatskii S I *The Origin of Cosmic Rays* (Oxford: Pergamon Press, 1964); Translated from Russian: *Proiskhozhdenie Kosmicheskikh Luchei* (Moscow: Izd. AN SSSR, 1963)
15. Ginzburg V L, Syrovatskii S I *Annu. Rev. Astron. Astrophys.* **3** 297 (1965)
16. Bühler R, Blandford R *Rep. Prog. Phys.* **77** 066901 (2014)
17. Pshirkov M S et al. *Mon. Not. R. Astron. Soc.* **496** 5227 (2020)
18. Fermi E *Phys. Rev.* **75** 1169 (1949)
19. Alfvén H *Cosmical Electrodynamics* (Oxford: Clarendon Press, 1950); Translated into Russian: *Kosmicheskaya Elektrodinamika* (Moscow: IL, 1952)
20. Syrovatskii S I *Usp. Fiz. Nauk* **62** 247 (1957)
21. Astapov I I et al. *J. Exp. Theor. Phys.* **134** 469 (2022); *Zh. Eksp. Teor. Fiz.* **161** 548 (2022)
22. Treumann R A *Astron. Astrophys. Rev.* **17** 409 (2009)
23. Bykov A M et al. *Astrophys. J.* **789** 137 (2014)
24. Ginzburg V L, Syrovatskii S I *Sov. Phys. Usp.* **7** 696 (1965); *Usp. Fiz. Nauk* **84** 201 (1964)
25. Dogiel V A, Ginzburg V L *Space Sci. Rev.* **49** 311 (1989)
26. Hillas A M *Cosmic Rays* (Amsterdam: Elsevier, 1972) https://doi.org/10.1016/C2013-0-02469-3
27. Axford W I, in *Origin of Cosmic Rays* (Intern. Astronomical Union Symp., Vol. 94, Eds G Setti, G Spada, A W Wolfendale) (Dordrecht: D. Reidel, 1981) p. 339, https://doi.org/10.1007/978-94-009-8475-2_57
28. Berezinskii V S et al. *Astrofizika Kosmicheskikh Luchei* (Astrophysics of Cosmic Rays) (Ed. V L Ginzburg) (Moscow: Nauka, 1984) translated into English, see [29]
29. Berezinskii V S et al. *Astrophysics of Cosmic Rays* (Ed. V L Ginzburg) (Amsterdam: North-Holland, 1990) original edition in Russian, see [28]
30. Hillas A M *J. Phys. G* **31** R95 (2005)
31. Amato E *Int. J. Mod. Phys. D* **23** 1430013 (2014)
32. Grenier I A, Black J H, Strong A W *Annu. Rev. Astron. Astrophys.* **53** 199 (2015)
33. Lingenfelter R E *Adv. Space Res.* **62** 2750 (2018)
34. Aguilar M et al. *Phys. Rep.* **894** 1 (2021)
35. Rankin J S et al. *Space Sci. Rev.* **218** (5) 42 (2022)
36. Panov A D, Podorozhnyi D M, Turundaevskii A N *Phys. Usp.* **67** 639 (2024); *Usp. Fiz. Nauk* **194** 681 (2024)
37. Alfaro R et al. *Astropart. Phys.* **167** 103077 (2025)
38. Kulikov G V, Khristiansen G B *Sov. Phys. JETP* **8** 441 (1959); *Zh. Eksp. Teor. Fiz.* **35** 635 (1958)
39. Cao Z et al. *Phys. Rev. Lett.* **132** 131002 (2024)
40. Zhen C et al. (The LHAASO Collab.), arXiv:2505.14447
41. Cao Z et al. *Nature* **594** 33 (2021)
42. Kuznetsov M Yu et al. *JCAP* **2024** (5) 125 (2024)
43. Abbasi R et al. *Astrophys. J.* **981** 182 (2025)
44. Cao Z et al. *Phys. Rev. Lett.* **131** 151001 (2023)
45. Vecchiotti V et al., arXiv:2411.11439
46. Espinosa Castro L E et al. *Mon. Not. R. Astron. Soc. Lett.* **543** L20 (2025); arXiv:2506.06593
47. Buitink S et al. *Nature* **531** 70 (2016)
48. Syrovatskii S I *Comm. Astrophys. Space Phys.* **3** 155 (1971)
49. Lemoine M, Waxman E *JCAP* **2009** (11) 009 (2009)
50. Margutti R et al. *Astrophys. J.* **797** 107 (2014)
51. Bykov A, Romansky V, Osipov S *Universe* **8** (1) 32 (2022)
52. Ma X-H et al. *Chinese Phys. C* **46** 030001 (2022)
53. Troitsky S V *Phys. Usp.* **67** 349 (2024); *Usp. Fiz. Nauk* **194** 371 (2024)
54. Lozinskaya T A *Supernovae and Stellar Wind in the Interstellar Medium* (New York: AIP, 1992); Translated from Russian: *Sverkhnovye Zvezdy i Zvezdnyi Veter: Vzaimodeistvie s Gazom Galaktiki* (Moscow: Nauka, 1986)
55. Branch D, Wheeler J C *Supernova Explosions* (Berlin: Springer-Verlag, 2017) https://doi.org/10.1007/978-3-662-55054-0
56. Vink J *Physics and Evolution of Supernova Remnants* (Cham: Springer, 2020) https://doi.org/10.1007/978-3-030-55231-2
57. Chevalier R A *Astrophys. J.* **619** 839 (2005)
58. Blinnikov S, in *Handbook of Supernovae* (Eds A W Alsabti, P Murdin) (Cham: Springer, 2017) p. 843, https://doi.org/10.1007/978-3-319-21846-5_31
59. Holland-Ashford T et al. *Astrophys. J.* **844** 84 (2017)
60. Baade W, Zwicky F *Proc. Natl. Acad. Sci. USA* **20** 254 (1934)
61. Imshennik V S, Nadezhin D K *Usp. Fiz. Nauk* **156** 561 (1988); *Sov. Sci. Rev. E* **8** (Pt. 1) 1 (1989)
62. Burrows A, Wang T, Vartanyan D *Astrophys. J. Lett.* **964** L16 (2024)
63. Choi L, Burrows A, Vartanyan D *Phys. Rev. D* **111** 123038 (2025); arXiv:2503.07531
64. Burrows A, Vartanyan D *Nature* **589** 29 (2021)
65. Nicholl M et al. *Nat. Astron.* **4** 893 (2020)
66. Adams S M et al. *Astrophys. J.* **778** 164 (2013)

[4] The simulations were performed jointly with S.M. Osipov, V.R. Romansky and Yu.A. Uvarov.

67. Quintana A L, Wright N J, Martínez García J *Mon. Not. R. Astron. Soc.* **538** 1367 (2025)
68. Bykov A M, Toptygin I N *Astrophys. Space Sci.* **138** 341 (1987)
69. Shukurov A, Subramanian K *Astrophysical Magnetic Fields*: *From Galaxies to the Early Universe* (Cambridge: Cambridge Univ. Press, 2021) https://doi.org/10.1017/9781139046657
70. Sarbadhicary S K et al. *Mon. Not. R. Astron. Soc.* **464** 2326 (2017)
71. Raymond J C et al. *Astrophys. J.* **888** 90 (2020)
72. Sunyaev R et al. *Astron. Astrophys.* **656** A132 (2021)
73. Churazov E M et al. *Mon. Not. R. Astron. Soc.* **513** L83 (2022)
74. van der Laan H *Mon. Not. R. Astron. Soc.* **124** 125 (1962)
75. Raymond J C et al. *Astrophys. J.* **894** 108 (2020)
76. Chomiuk L, Metzger B D, Shen K J *Annu. Rev. Astron. Astrophys.* **59** 391 (2021)
77. Shafter A W *Astrophys. J.* **834** 196 (2017)
78. H. E. S. S. Collab., Aharonian F et al. *Science* **376** 77 (2022)
79. López-Coto R et al. *Astron. Astrophys.* **696** A24 (2025)
80. Zirakashvili V N, Ptuskin V S *Astropart. Phys.* **78** 28 (2016)
81. Murase K *Phys. Rev. D* **97** 081301 (2018)
82. Murase K *Phys. Rev. D* **109** 103020 (2024)
83. Brose R, Sushch I, Mackey J *Astron. Astrophys.* **699** A160 (2025); arXiv:2504.20601
84. Chugai N N, Danziger I J *Mon. Not. R. Astron. Soc.* **268** 173 (1994)
85. Pessi P J et al. *Astron. Astrophys.* **695** A142 (2025)
86. Martí-Devesa G et al. *Astron. Astrophys.* **686** A254 (2024)
87. Jacobson-Galán W V et al., arXiv:2505.04698; *Astrophys. J.* (2025) submitted
88. Waxman E et al. *Astrophys. J.* **978** 133 (2025)
89. Gal-Yam A et al. *Astrophys. J.* **639** 331 (2006)
90. Soderberg A M et al. *Nature* **463** 513 (2010)
91. Chakraborti S et al. *Nat. Commun.* **2** 175 (2011)
92. Margutti R et al. *Astrophys. J.* **797** 107 (2014)
93. Bykov A M *Phys. Usp.* **61** 805 (2018); *Usp. Fiz. Nauk* **188** 894 (2018)
94. Wang X-Y et al. *Phys. Rev. D* **76** 083009 (2007)
95. Budnik R et al. *Astrophys. J.* **673** 928 (2008)
96. Bykov A M et al. *Space Sci. Rev.* **214** 41 (2018)
97. Bykov A M, Osipov S M, Romanskii V I *J. Exp. Theor. Phys.* **134** 487 (2022); *Zh. Eksp. Teor. Fiz.* **161** 570 (2022)
98. Romansky V I, Bykov A M, Osipov S M *Adv. Space Res.* **74** 4290 (2024)
99. Levinson A, Nakar E *Phys. Rep.* **866** 1 (2020)
100. Sagdeev R Z, in *Plasma Physics and the Problem of Controlled Thermonuclear Reactions* Vol. 4 (Ed. M A Leontovich) (New York: Pergamon Press, 1961) p. 454; Translated from Russian: in *Fizika Plazmy i Problema Termoyadernykh Reaktsii* (Moscow: Izd. AN SSSR, 1958) p. 384
101. Kennel C F, Edmiston J P, Hada T, in *Collisionless Shocks in the Heliosphere*: *A Tutorial Review* (Geophysical Monograph Ser., Vol. 34, Eds R G Stone, B T Tsurutani) (Washington, DC: American Geophysical Union, 1985) p. 1
102. Sagdeev R Z *Izbrannye Trudy* (Selected Works) Vol. 1 *Fizika Plazmy i Upravlyaemyi Termoyadernyi Sintez* (Plasma Physics and Controlled Fusion) (Novosibirsk: IPTs NGU, 2024)
103. Balogh A, Treumann R A *Physics of Collisionless Shocks*: *Space Plasma Shock Waves* (New York: Springer, 2013) https://doi.org/10.1007/978-1-4614-6099-2
104. Bykov A M, Treumann R A *Astron. Astrophys. Rev.* **19** 42 (2011)
105. Burgess D, Scholer M *Collisionless Shocks in Space Plasmas* (Cambridge: Cambridge Univ. Press, 2015) https://doi.org/10.1017/CBO9781139044097
106. Marcowith A et al. *Rep. Prog. Phys.* **79** 046901 (2016)
107. Hockney R W, Eastwood J W *Computer Simulation Using Particles* (New York: McGraw-Hill, 1981); Translated into Russian: *Chislennoe Modelirovanie Metodom Chastits* (Moscow: Mir, 1987)
108. Lipatov A S *The Hybrid Multiscale Simulation Technology*: *An Introduction with Application to Astrophysical and Laboratory Plasmas* (Berlin: Springer, 2002) https://doi.org/10.1007/978-3-662-05012-5
109. Grigor'ev Yu N, Vshivkov V A, Fedoruk M P *Chislennoe Modelirovanie Metodami Chastits-v-Yacheikakh* (Numerical Simulation by Particle-in-Cell Methods) (Novosibirsk: Izd. SO RAN, 2004)
110. Jones F C, Jokipii J R, Baring M G *Astrophys. J.* **509** 238 (1998)
111. Spitkovsky A *Astrophys. J. Lett.* **682** L5 (2008)
112. Sironi L, Spitkovsky A, Arons J *Astrophys. J.* **771** 54 (2013)
113. Pohl M, Hoshino M, Niemiec J *Prog. Part. Nucl. Phys.* **111** 103751 (2020)
114. Crumley P et al. *Mon. Not. R. Astron. Soc.* **485** 5105 (2019)
115. Romansky V I, Bykov A M, Osipov S M *J. Phys. Conf. Ser.* **1400** 022005 (2019)
116. Hoshino M, in *Space and Astrophysical Plasma Simulation. Methods, Algorithms, and Applications* (Ed. J Büchner) (Cham: Springer, 2023) p. 337, https://doi.org/10.1007/978-3-031-11870-8_11
117. Chakraborti S et al. *Nat. Commun.* **2** 175 (2011)
118. Churazov E M, Khabibullin I I, Bykov A M *Astron. Astrophys.* **688** A4 (2024)
119. Cherepashchuk A M, Dodin A V, Postnov K A *Phys. Usp.* **68** (2025) https://doi.org/10.3367/UFNe.2025.05.039904, in press; *Usp. Fiz. Nauk* **195** (2025) https://doi.org/10.3367/UFNr.2025.05.039904, in press; arXiv:2506.01106
120. Winske D et al., in *Space and Astrophysical Plasma Simulation. Methods, Algorithms, and Applications* (Ed. J Büchner) (Cham: Springer, 2023) p. 63, https://doi.org/10.1007/978-3-031-11870-8_3
121. Burgess D et al. *J. Plasma Phys.* **82** 905820401 (2016)
122. Kropotina J A et al. *Mon. Not. R. Astron. Soc.* **524** 2934 (2023)
123. Kropotina Yu A et al. *Tech. Phys.* **61** 517 (2016); *Zh. Tekh. Fiz.* **86** (4) 40 (2016)
124. Bykov A M, Uvarov Yu A *J. Exp. Theor. Phys.* **88** 465 (1999); *Zh. Eksp. Teor. Fiz.* **115** 846 (1999)
125. Park J, Caprioli D, Spitkovsky A *Phys. Rev. Lett.* **114** 085003 (2015)
126. van Marle A J et al. *Astrophys. J.* **929** 7 (2022)
127. Berezhko E G, Elshin V K, Ksenofontov L T *J. Exp. Theor. Phys.* **82** 1 (1996); *Zh. Eksp. Teor. Fiz.* **109** (1) 3 (1996)
128. Zirakashvili V N, Ptuskin V S *Astropart. Phys.* **39–40** 12 (2012)
129. Schwartz S J, Skilling J *Astron. Astrophys.* **70** 607 (1978)
130. Ptuskin V S, Zirakashvili V N *Adv. Space Res.* **37** 1898 (2006)
131. Ellison D C, Bykov A M *Astrophys. J.* **731** 87 (2011)
132. Drury L O *Mon. Not. R. Astron. Soc.* **415** 1807 (2011)
133. Marcowith A *Front. Astron. Space Sci.* **11** 1411076 (2025)
134. Neronov A, Malyshev D, Semikoz D V *Astron. Astrophys.* **606** A22 (2017)
135. Aharonian F et al. *Space Sci. Rev.* **166** 97 (2012)
136. Moskalenko I V, Strong A W, Reimer O *Astron. Astrophys.* **338** L75 (1998)
137. Porter T A, Jóhannesson G, Moskalenko I V *Astrophys. J. Suppl.* **262** (1) 30 (2022)
138. Syrovatskii S I *Annu. Rev. Astron. Astrophys.* **19** 163 (1981)
139. Syrovatskii S I, Bulanov S V, Dogiel V A *Itogi Nauki i Tekhniki* (Results of Science and Technology) (Ser. Astronomy) Vol. 21 (Moscow: VINITI, 1982) p. 188
140. Zelenyi L M et al. *Phys. Usp.* **53** 933 (2010); *Usp. Fiz. Nauk* **180** 973 (2010)
141. Birn J et al. *Space Sci. Rev.* **173** 49 (2012)
142. Artemyev A et al. *Astrophys. J.* **923** 151 (2021)
143. Arons J *Space Sci. Rev.* **173** 341 (2012)
144. Zrake J *Astrophys. J.* **823** 39 (2016)
145. Fermi E *Astrophys. J.* **119** 1 (1954)
146. Blandford R, Eichler D *Phys. Rep.* **154** 1 (1987)
147. Lemoine M *Phys. Rev. Lett.* **129** 215101 (2022)
148. Hoshino M *Phys. Plasmas* **31** 052901 (2024)
149. Ulam S M, in *Proc. of the Fourth Berkeley Symp. on Mathematical Statistics and Probability, Univ. of California, June 20–July 30, 1960* Vol. 3 (Ed. J Neyman) (Berkeley, CA: Univ. of California Press, 1961) p. 315
150. Zaslavskii G M, Chirikov B V *Sov. Phys. Dokl.* **9** 989 (1965); *Dokl. Akad. Nauk SSSR* **159** 306 (1964)
151. Zaslavskii G M, Chirkov B V *Sov. Phys. Usp.* **14** 549 (1971); *Usp. Fiz. Nauk* **105** 3 (1971)
152. Lieberman M A, Lichtenberg A J *Phys. Rev. A* **5** 1852 (1972)
153. Lichtenberg A J, Lieberman M A *Regular and Chaotic Dynamics* (New York: Springer, 1992) https://doi.org/10.1007/978-1-4757-2184-3
154. Krymskii G F *Sov. Phys. Dokl.* **22** 327 (1977); *Dokl. Akad. Nauk SSSR* **234** 1306 (1977)
155. Bell A R *Mon. Not. R. Astron. Soc.* **182** 147 (1978)
156. Axford W I, Leer E, Skadron G, in *Proc. of the 15th Intern. Cosmic Ray Conf., Plovdiv* Vol. 11 (Budapest: Dept. of Cosmic Rays,

Central Research Institute for Physics of the Hungarian Academy of Sciences, 1977) p. 132
157. Blandford R D, Ostriker J P *Astrophys. J.* **221** L29 (1978)
158. Jones F C *Astrophys. J. Suppl.* **90** 561 (1994)
159. Berezhko E G, Krymskii G F *Sov. Phys. Usp.* **31** 27 (1988); *Usp. Fiz. Nauk* **154** 49 (1988)
160. Jones F C, Ellison D C *Space Sci. Rev.* **58** 259 (1991)
161. Zel'dovich Ya B, Raizer Yu P *Physics of Shock Waves and High-Temperature Hydrodynamic Phenomena* (Mineola, NY: Dover Publ., 2002); Translated from Russian: *Fizika Udarnykh Voln i Vysokotemperaturnykh Gidrodinamicheskikh Yavlenii* (Moscow: Nauka, 1966)
162. Waxman E, Katz B, in *Handbook of Supernovae* (Eds A W Alsabti, P Murdin) (Cham: Springer, 2017) p. 967, https://doi.org/10.1007/978-3-319-21846-5_33
163. Vladimirov A E, Bykov A M, Ellison D C *Astrophys. J.* **688** 1084 (2008)
164. Ellison D C, Eichler D *Astrophys. J.* **286** 691 (1984)
165. Ellison D C, Moebius E, Paschmann G *Astrophys. J.* **352** 376 (1990)
166. Vladimirov A, Ph.D. Thesis (Raleigh, NC: North Carolina State Univ., 2009)
167. Ellison D C, Warren D C, Bykov A M *Astrophys. J.* **776** 46 (2013)
168. Berezinskii V S et al. *Astrofizika Kosmicheskikh Luchei* (Astrophysics of Cosmic Rays) (Ed. V L Ginzburg) (Moscow: Nauka, 1990) translated into English, see [29]
169. Schure K M et al. *Space Sci. Rev.* **173** 491 (2012)
170. Bykov A M et al. *Space Sci. Rev.* **178** 201 (2013)
171. Bell A R *Mon. Not. R. Astron. Soc.* **353** 550 (2004)
172. Ginzburg V L, Syrovatskii S I *Sov. Phys. JETP* **18** 245 (1964); *Zh. Eksp. Teor. Fiz.* **45** 353 (1963)
173. Reynolds S P, Chevalier R A *Astrophys. J.* **245** 912 (1981)
174. Helder E A et al. *Space Sci. Rev.* **173** 369 (2012)
175. Reed J E et al. *Astrophys. J.* **440** 706 (1995)
176. Slane P et al. *Galaxies* **12** (5) 59 (2024)
177. Mercuri A et al. *Astrophys. J.* **986** 6 (2025)
178. Ferrazzoli R et al. *Astrophys. J.* **945** 52 (2023)
179. Zhou P et al. *Astrophys. J.* **957** 55 (2023)
180. Ferrazzoli R et al. *Astrophys. J.* **967** L38 (2024)
181. Zirakashvili V N, Ptuskin V S *Astrophys. J.* **678** 939 (2008)
182. Bykov A M et al. *Phys. Rev. D* **110** 023041 (2024)
183. Aharonian F A *Very High Energy Cosmic Gamma Radiation: A Crucial Window on the Extreme Universe* (Singapore: World Scientific Publ., 2004)
184. Funk S *Annu. Rev. Nucl. Part. Sci* **65** 245 (2015)
185. Slane P et al. *Space Sci. Rev.* **188** 187 (2015)
186. Yang R Z, Kafexhiu E, Aharonian F *Astron. Astrophys.* **615** A108 (2018)
187. Giuliani A et al. *Astrophys. J.* **742** L30 (2011)
188. Ackermann M et al. *Science* **339** 807 (2013)
189. Aharonian F et al. *Astron. Astrophys.* **464** 235 (2007)
190. Ellison D C et al. *Astrophys. J.* **744** 39 (2012)
191. Tsuji N et al. *Astrophys. J.* **877** 96 (2019)
192. Fukui Y et al. *Astrophys. J.* **961** 162 (2024)
193. Reynolds S P et al. *Astrophys. J.* **695** L149 (2009)
194. Aharonian F, Sun X, Yang R *Astron. Astrophys.* **603** A7 (2017)
195. Cao Z et al. *Astrophys. J.* **982** L33 (2025)
196. Archambault S et al. *Astrophys. J.* **836** 23 (2017)
197. Wilhelm A et al. *Astron. Astrophys.* **639** A124 (2020)
198. Aharonian F A *Astropart. Phys.* **43** 71 (2013)
199. Ptuskin V, Zirakashvili V, Seo E S *Astrophys. J.* **718** 31 (2010)
200. Schure K M, Bell A R *Mon. Not. R. Astron. Soc.* **435** 1174 (2013)
201. Alfaro R et al., arXiv:2503.20947
202. Bykov A M et al. *Adv. Space Res.* **74** 4276 (2024)
203. LHAASO Collab., arXiv:2410.08988
204. Abeysekara A U et al. *Nature* **562** 82 (2018)
205. H. E. S. S. Collab., Aharonian F et al. *Science* **383** 402 (2024)
206. Alfaro R et al. *Astrophys. J.* **976** 30 (2024)
207. Safi-Harb S et al. *Astrophys. J.* **935** 163 (2022)
208. Kaaret P et al. *Astrophys. J. Lett.* **961** L12 (2024)
209. Kuzmichev L A *Phys. Part Nucl.* **56** 297 (2025); *Fiz. Elem. Chastits Atom. Yadra* **56** 469 (2025)